Detection, Estimation, and Modulation Theory, Part III: Radar–Sonar Signal Processing and Gaussian Signals in Noise. Harry L. Van Trees

ISBNs: 0-471-10793-X (Paperback); 0-471-22109-0 (Electronic)

4

Special Categories of Detection Problems

In Chapters 2 and 3, we studied the simple binary detection problem and the general binary detection problem. Most of our examples dealt with state-representable processes, because we could obtain a complete solution for this class of problem. In this chapter, we discuss three categories of problems for which we can also obtain a complete solution. The three categories are the following:

1. The stationary-processes, long-observation-time (SPLOT) problem.
2. The separable-kernel (SK) problem.
3. The low-energy-coherence (LEC) problem.

We shall explain the categories in detail in the appropriate sections. The discussion is important for two reasons. First, almost all physical situations fall into one of these four categories (the above three categories plus finite-state processes). Second, we can obtain a complete solution for problems in these categories.

4.1 STATIONARY PROCESSES: LONG OBSERVATION TIME

In many physical situations of interest, the received waveforms under both hypotheses are segments of stationary processes. Thus, we can characterize the processes by their power density spectra. If the spectra are rational, they will have a finite-dimensional state representation and we can solve the problem using state-variable techniques. In our previous work with state variables we saw that when the input was a stationary process the gains in the optimum system approached constant values and the system approached a time-invariant system. In this section, we consider

cases in which the observation time is *long* compared with the time necessary for the system transients to decay. By ignoring the transient, we can obtain much simpler solutions. If desired, we can always check the validity of the approximation by solving the problem with state-variable techniques. We refer to the results obtained by ignoring the transients as asymptotic results and add a subscript ∞ to the various expressions. As in the general case, we are interested in optimum receiver structures and their performance. We begin our discussion with the simple binary problem.

4.1.1 Simple Binary Problem

The model for the simple binary problem was given in Section 2.1. For algebraic simplicity we discuss only the zero-mean case in the text. The received waveforms are

$$\begin{aligned} r(t) &= s(t) + w(t), \qquad T_i \leq t \leq T_f: H_1, \\ r(t) &= w(t), \qquad\quad T_i \leq t \leq T_f: H_0, \end{aligned} \tag{1}$$

We assume that $s(t)$ is a zero-mean Gaussian process with spectrum $S_s(\omega)$. The noise $w(t)$ is a white, zero-mean Gaussian process that is statistically independent of $s(t)$ and has a spectral height $N_0/2$. The LRT is

$$l_R + l_B \underset{H_0}{\overset{H_1}{\gtrless}} \ln \eta. \tag{2}$$

We first examine various receiver realizations for computing l_R. Next we derive a formula for l_B. Finally, we compute the performance.

If we use Canonical Realization No. 1 (pages 15–16),

$$l_R = \frac{1}{N_0} \int_{T_i}^{T_f} \int r(t) h_1(t, u) r(u)\, dt\, du, \tag{3}$$

where $h_1(t, u)$ is a solution to (4),

$$\frac{N_0}{2} h_1(t, u) + \int_{T_i}^{T_f} h_1(t, z) K_s(z - u)\, dz = K_s(t - u), \qquad T_i \leq t, u \leq T_f. \tag{4}$$

From our work in Chapter I-4 (page I-321), we know that the total solution is made up of a particular solution that does not depend on the limits and a weighted sum of bounded homogeneous solutions that give the correct endpoint conditions. These homogeneous solutions decay as we move into the interior of the interval. If the time interval is large, the particular solution will exert the most influence on l_R, so that we can

obtain a good approximation to the solution by neglecting the homogeneous solutions. To accomplish this, we let $T_i = -\infty$ and $T_f = \infty$ in (4). With the infinite limits, we would assume that we could find a solution to (4) that corresponded to a time-invariant filter. To verify this, we let

$$h_1(t, u) = h_{1\infty}(t - u) \tag{5}$$

in (4) and try to find a solution. Rewriting (4), we have

$$\frac{N_0}{2} h_{1\infty}(t - u) + \int_{-\infty}^{\infty} h_{1\infty}(t - z)K_s(z - u)\, dz = K_s(t - u), \qquad -\infty < t, u < \infty, \tag{6}$$

which can be solved by using Fourier transforms. Transforming, we have

$$\boxed{H_{1\infty}(j\omega) = \frac{S_s(\omega)}{S_s(\omega) + (N_0/2)},} \tag{7}$$

which is the desired result. This filter is familiar from our work with unrealizable MMSE estimators in Section I-6.2.3. The resulting receiver is shown in Fig. 4.1. Notice that we have used only the infinite limits to solve the integral equation. The receiver still operates on $r(t)$ over $[T_i, T_f]$.

To implement Canonical Realization No. 3, we must solve (2.45).

$$h_1(t, u) = \int_{T_i}^{T_f} h_f(z, t)h_f(z, u)\, dz, \qquad T_i \leq t, u \leq T_f. \tag{8}$$

To find the asymptotic solution, we let $T_i = -\infty$ and $T_f = \infty$, use (5), and assume that a time-invariant solution exists. The resulting equation is

$$h_{1\infty}(t - u) = \int_{-\infty}^{\infty} h_{f\infty}(z - t)h_{f\infty}(z - u)\, dz, \qquad -\infty < t, u < \infty. \tag{9}$$

Transforming, we have

$$H_{1\infty}(j\omega) = |H_{f\infty}(j\omega)|^2. \tag{10}$$

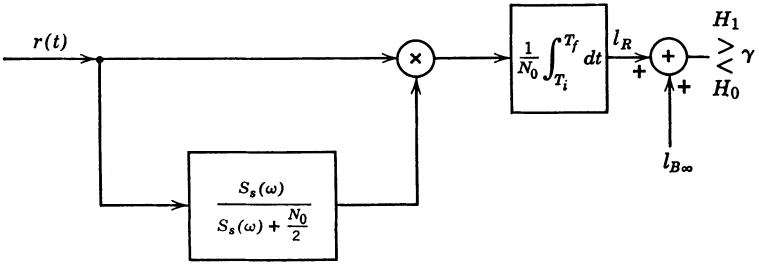

Fig. 4.1 Canonical Receiver No. 1: stationary process, long observation time.

This type of equation is familiar from our spectrum factorization work in Section I-6.2. Because $H_{1\infty}(j\omega)$ has all the properties of a power density spectrum, we can obtain a realizable solution easily.

$$\boxed{H_{fr\infty}(j\omega) = [H_{1\infty}(j\omega)]^{+}.} \tag{11}$$

We recall that the superscript + means that we assign all the poles and zeros of $H_{1\infty}(s)$ that lie in the left half of the complex s-plane to $H_{fr\infty}(s)$. Notice that this assignment of zeros is somewhat arbitrary. (Recall the discussion on page I-311.) Thus the solution to (10) that we have indicated in (11) is not unique. The resulting receiver is shown in Fig. 4.2. Notice that we can also choose an unrealizable solution to (10). An example is

$$H_{fu\infty}(j\omega) = |H_{1\infty}(j\omega)|^{1/2}. \tag{12}$$

To implement Canonical Realization No. 4, we must solve the realizable filtering problem. By letting $T_i = -\infty$ and assuming stationarity, we obtain the Wiener filtering problem. The solution is given by (I-6.78),

$$H_{or\infty}(j\omega) = \frac{1}{[S_s(\omega) + (N_0/2)]^{+}} \left[\frac{S_s(\omega)}{[S_s(\omega) + (N_0/2)]^{-}} \right]_{+}. \tag{13}$$

The receiver is shown in Fig. 4.3. Comparing Figs. 4.1, 4.2, and 4.3, we see that Canonical Realization No. 3 in Fig. 4.2 is the simplest to implement.

To evaluate the bias l_B, we begin with (2.73).

$$l_B = -\frac{1}{N_0} \int_{T_i}^{T_f} \xi_{Ps}(t)\, dt, \tag{14}$$

where $\xi_{Ps}(t)$ is the realizable mean-square error in estimating $s(t)$, assuming that H_1 is true. In our work in Section I-6.3 (particularly Examples 1 and 2 on pages I-546–I-555), we saw that $\xi_{Ps}(t)$ approached the steady-state, mean-square error, $\xi_{P\infty}$, reasonably quickly. Thus, if $T_f - T_i \triangleq T$ is long compared to the length of this initial transient, we can obtain a good approximation to l_B by replacing $\xi_{Ps}(t)$ with $\xi_{P\infty}$.

$$l_{B\infty} \triangleq -\frac{1}{N_0} \int_{T_i}^{T_f} \xi_{P\infty}\, dt = -\frac{T}{N_0}\, \xi_{P\infty}. \tag{15}$$

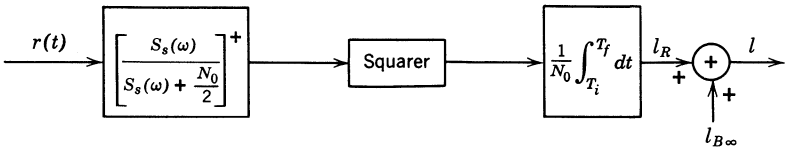

Fig. 4.2 Canonical Receiver No. 3: stationary process, long observation time.

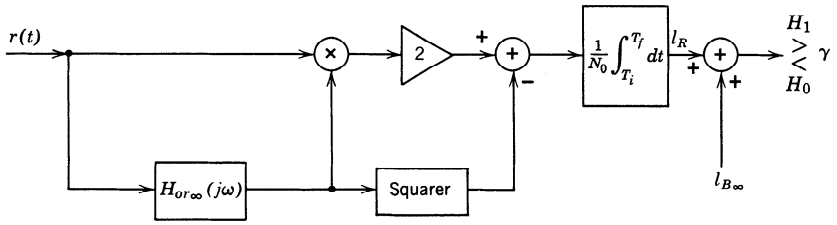

Fig. 4.3 Canonical Realization No. 4: stationary process, long observation time.

In Section I-6.2.4 we derived a closed-form expression for $\xi_{P\infty}$. From (I-6.152),

$$\boxed{\xi_{P\infty} = \frac{N_0}{2}\int_{-\infty}^{\infty} \ln\left[1 + \frac{S_s(\omega)}{N_0/2}\right]\frac{d\omega}{2\pi}.} \tag{16}$$

Using (16) in (15) gives

$$\boxed{l_{B\infty} = -\frac{T}{2}\int_{-\infty}^{\infty} \ln\left[1 + \frac{S_s(\omega)}{N_0/2}\right]\frac{d\omega}{2\pi},} \tag{17}$$

where

$$T \triangleq T_f - T_i. \tag{18}$$

The result in (17) can also be obtained directly from the asymptotic value of the logarithm of the Fredholm determinant in (2.74) [e.g., page I-207 (I-3.182)].

An identical argument gives the asymptotic form of $\mu(s)$, which we denote by $\mu_\infty(s)$. From (2.138),

$$\mu(s) = \frac{1-s}{N_0}\int_{T_i}^{T_f} dt\left\{\xi_P\left(t \mid s(\cdot), \frac{N_0}{2}\right) - \xi_P\left(t \mid s(\cdot), \frac{N_0}{2(1-s)}\right)\right\}. \tag{19}$$

(Notice that $\mu(s) = \mu_R(s)$ because of the zero mean assumption.) Replacing $\xi_P(t \mid s(\cdot), \cdot)$ by $\xi_{P\infty}(s(\cdot), \cdot)$, we have

$$\boxed{\mu_\infty(s) = \frac{(1-s)T}{N_0}\left\{\xi_{P\infty}\left(s(\cdot), \frac{N_0}{2}\right) - \xi_{P\infty}\left(s(\cdot), \frac{N_0}{2(1-s)}\right)\right\}.} \tag{20}$$

Using (16), we obtain

$$\boxed{\begin{aligned}\mu_\infty(s) = \frac{T}{2}\Bigg\{&(1-s)\int_{-\infty}^{\infty} \ln\left[1 + \frac{2S_s(\omega)}{N_0}\right]\frac{d\omega}{2\pi} \\ &- \int_{-\infty}^{\infty} \ln\left[1 + \frac{2(1-s)S_s(\omega)}{N_0}\right]\frac{d\omega}{2\pi}\Bigg\}.\end{aligned}} \tag{21}$$

An equivalent form is

$$\mu_\infty(s) = \frac{T}{2}\int_{-\infty}^{\infty} \ln\left[\frac{[1 + (2S_s(\omega)/N_0)]^{1-s}}{[1 + (2(1-s)S_s(\omega)/N_0)]}\right]\frac{d\omega}{2\pi} \tag{22}$$

To illustrate the application of these asymptotic results, we consider two simple examples.

Example 1. First-Order Butterworth Spectrum. The received waveforms on the two hypotheses are

$$\begin{aligned} r(t) &= s(t) + w(t), \qquad T_i \le t \le T_f: H_1, \\ r(t) &= w(t), \qquad\quad T_i \le t \le T_f: H_0. \end{aligned} \tag{23}$$

The signal process, $s(t)$, is a sample function from a stationary, zero-mean, Gaussian random process with spectrum $S_s(\omega)$,

$$S_s(\omega) = \frac{2kP}{\omega^2 + k^2}, \qquad -\infty < \omega < \infty. \tag{24}$$

The noise process is a statistically independent, zero-mean white Gaussian random process with spectral height $N_0/2$.

We shall use Canonical Realization No. 3 (Fig. 4.2) for the receiver. Using (24) in (7), we obtain

$$H_{1\infty}(j\omega) = \frac{2kP/(\omega^2 + k^2)}{(2kP/(\omega^2 + k^2)) + N_0/2} = \frac{k^2\Lambda_1}{[\omega^2 + k^2(1 + \Lambda_1)]}, \tag{25}$$

where

$$\Lambda_1 = \frac{4P}{kN_0} \tag{26}$$

is the signal-to-noise ratio in the message bandwidth. From (11),

$$H_{f\infty}(j\omega) = [H_{1\infty}(j\omega)]^+ = \frac{k\Lambda_1^{1/2}}{j\omega + k\sqrt{1 + \Lambda_1}}. \tag{27}$$

We obtain the bias term from (15). The mean-square error $\xi_{P\infty}$ was evaluated for the first-order Butterworth spectrum in Example 3 on page I-495. From (I-6.112),

$$\xi_{P\infty} = \frac{2P}{1 + \sqrt{1 + \Lambda_1}}. \tag{28}$$

Using (28) in (15), we have

$$l_{B\infty} = -\frac{2PT}{N_0[1 + \sqrt{1 + \Lambda_1}]}. \tag{29}$$

The resulting receiver is shown in Fig. 4.4. By incorporating part of the filter gain in the integrator, we can implement the filter as a simple resistor-capacitor circuit. Notice that the location of the pole of the filter depends on Λ_1. As Λ_1 decreases, the filter pole approaches the pole of the message spectrum. As Λ_1 increases, the bandwidth of the filter increases.

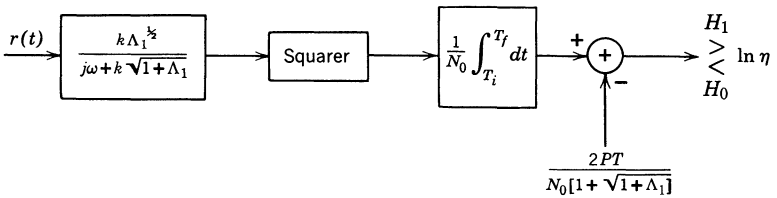

Fig. 4.4 Filter-squarer receiver: first-order Butterworth spectrum, long observation time.

To evaluate the performance, we find $\mu_\infty(s)$ by using (28) in (20).

$$\mu_\infty(s) = \frac{(1-s)T}{N_0}\left\{\frac{2P}{1+\sqrt{1+\Lambda_1}} - \frac{2P}{1+\sqrt{1+(1-s)\Lambda_1}}\right\}. \tag{30}$$

At this point it is useful to introduce an efficient notation to emphasize the important parameters in the performance expression.

We introduce several quantities,

$$\bar{E}_r \triangleq PT, \tag{31}$$

which is the average energy in the signal process, and

$$D_1 \triangleq \frac{kT}{2}, \tag{32}$$

which is a measure of the time-bandwidth product of the signal process. Notice that

$$\Lambda_1 = \frac{2\bar{E}_r/N_0}{D_1}. \tag{33}$$

Using (31) in (30), we obtain

$$\mu_\infty(s) = -\left(\frac{2\bar{E}_r}{N_0}\right) g_1(s, \Lambda_1), \tag{34}$$

where

$$g_1(s, \Lambda_1) \triangleq -(1-s)\{(1+\sqrt{1+\Lambda_1})^{-1} - (1+\sqrt{1+(1-s)\Lambda_1})^{-1}\}. \tag{35}$$

The first factor in (34) is the average signal energy-to-noise ratio and appears in all detection problems. The second term includes the effect of the spectral shape, the signal-to-noise ratio in the message bandwidth, and the threshold. It is this term that will vary in different examples. To evaluate the approximate expressions for P_F and P_D, we need $\dot{\mu}_\infty(s)$ and $\ddot{\mu}_\infty(s)$. Then, from (2.166) and (2.174),

$$P_F \simeq \frac{1}{\sqrt{2\pi s^2 \ddot{\mu}_\infty(s)}} \exp\left[\mu_\infty(s) - s\dot{\mu}_\infty(s)\right] \tag{36}$$

and

$$P_M \simeq \frac{1}{\sqrt{2\pi(1-s)^2 \ddot{\mu}_\infty(s)}} \exp\left[\mu_\infty(s) + (1-s)\dot{\mu}_\infty(s)\right] \tag{37}$$

From (34) and (35) we can obtain the necessary quantities to substitute into (36) and (37). In Figs. 4.5–4.7 we have plotted the approximate performance characteristics

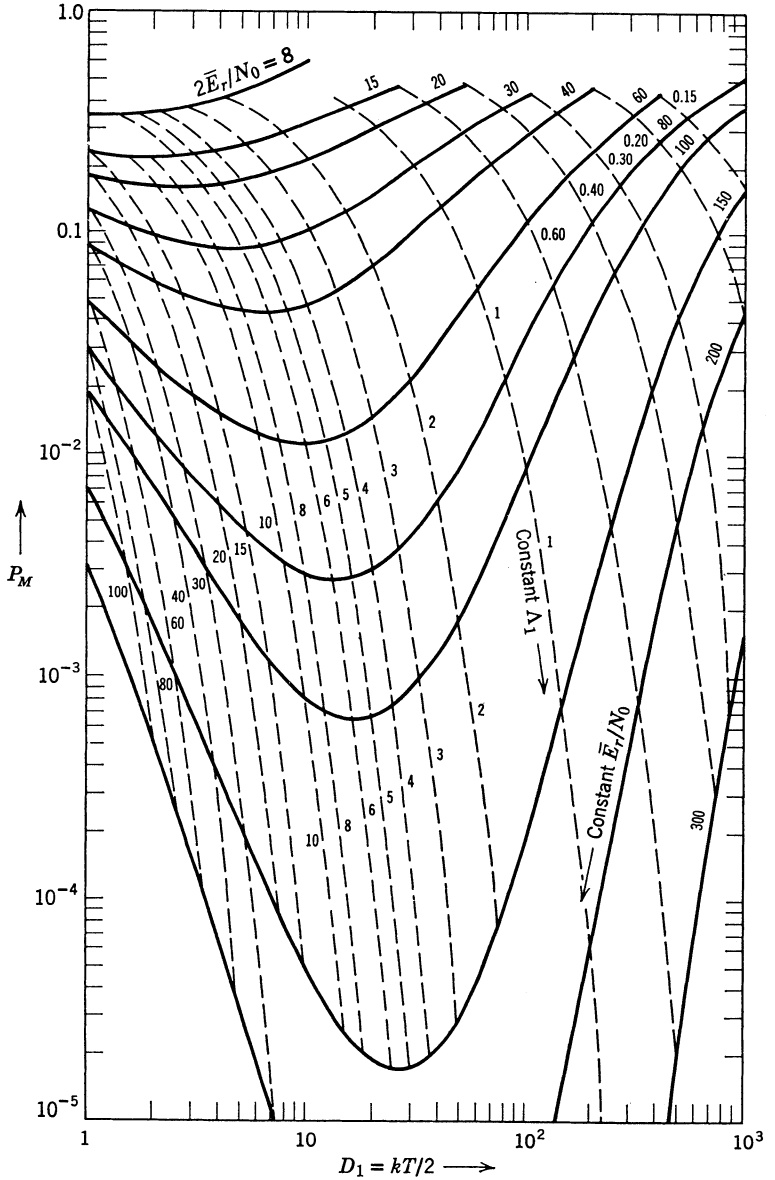

Fig. 4.5 Probability of miss versus time-bandwidth product: first-order Butterworth spectrum, $P_F = 10^{-1}$.

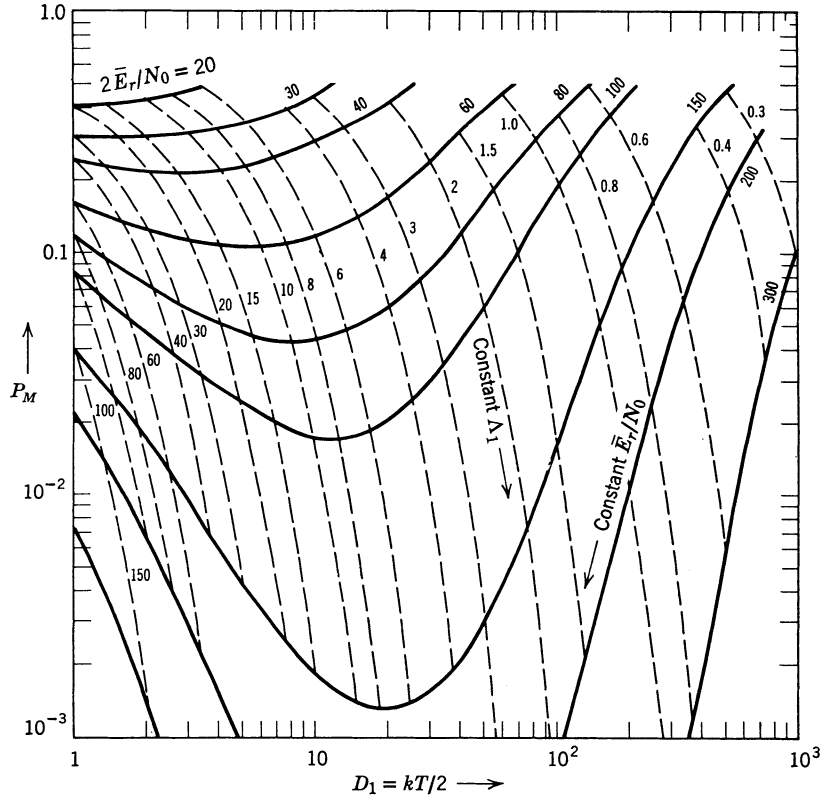

Fig. 4.6 Probability of miss versus time-bandwidth product for first-order Butterworth spectrum, $P_F = 10^{-3}$.

indicated by (36) and (37). In Fig. 4.5 we have constrained P_F to equal 10^{-1}. The horizontal axis is D_1 ($= kT/2$). The vertical axis is P_M. The solid curves correspond to constant values of $2\bar{E}_r/N_0$. We see that the performance is strongly dependent on the time-bandwidth product of the signal process. Notice that there is an optimum value of Λ_1 for each value of $2\bar{E}_r/N_0$. This optimum value is in the vicinity of $\Lambda_1 = 6$. (We shall find the exact minimum in a later example.) The dashed curves correspond to constant values of Λ_1. Moving to the right on a constant Λ_1 curve corresponds physically to increasing the observation time. Similar results are shown for $P_F = 10^{-3}$ and $P_F = 10^{-5}$ in Figs. 4.6 and 4.7, respectively.

For small values of D_1 (say, $D_1 < 2$), the curves should be checked using state-variable techniques, because the SPLOT approximation may not be valid.

For larger time-bandwidth products our performance calculations give good results, for two reasons:

1. The error resulting from the large time-interval approximation decreases rapidly as kT increases. We shall make some quantitative statements about the error on page 142.

2. The error resulting from truncating the Edgeworth series at the first term decreases as kT increases, because there are more significant eigenvalues. As the number of

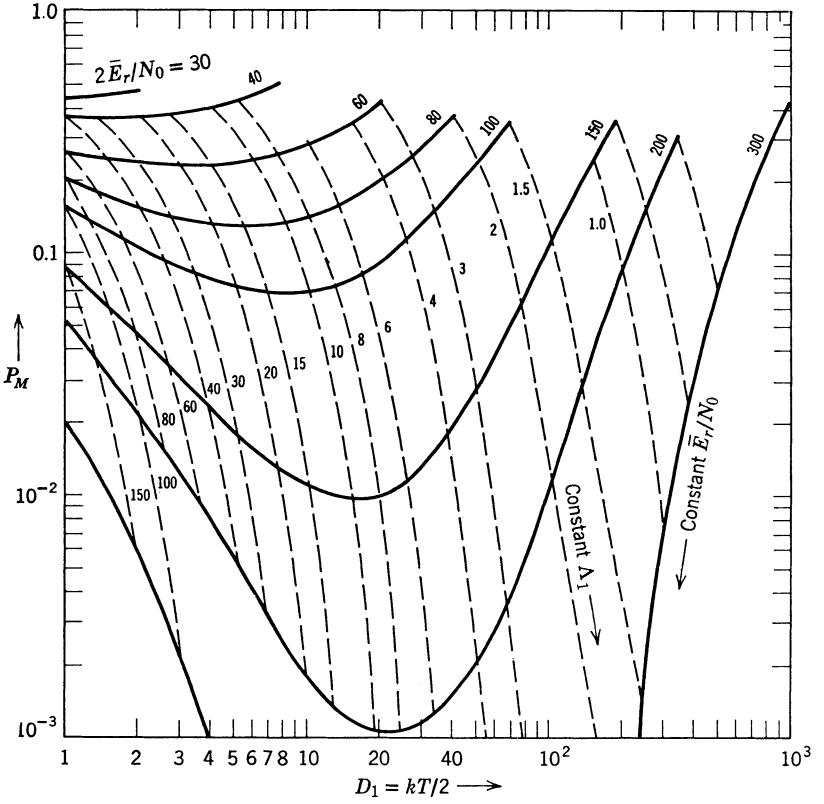

Fig. 4.7 Probability of miss versus time-bandwidth product for first-order Butterworth spectrum, $P_F = 10^{-5}$.

significant eigenvalues increases, the tilted density becomes closer to a Gaussian density.

Notice that if the system is operating close to the optimum value of Λ_1, D_1 will be large enough to make the SPLOT approximation valid.

Similar results for higher-order Butterworth spectra can be obtained easily (see Problem 4.1.3). In the next example we consider the case in which the signal has an ideal bandlimited message spectrum. This is a problem that is difficult to treat using state-variable techniques but is straightforward when the SPLOT condition is valid.

Example 2. In this example, we assume that $S_s(\omega)$ has a bandlimited spectrum

$$S_s(\omega) = \begin{cases} \dfrac{P}{2W}, & -2\pi W \leq \omega \leq 2\pi W, \\ 0, & \text{elsewhere.} \end{cases} \tag{38}$$

The most practical receiver configuration is No. 3. From (38) and (7),

$$H_{1\infty}(j\omega) = \begin{cases} \dfrac{P}{P + N_0 W}, & -2\pi W \leq \omega \leq 2\pi W, \\ 0, & \text{elsewhere.} \end{cases} \tag{39}$$

Thus,

$$H_{fu\infty}(j\omega) = \begin{cases} \dfrac{1}{(1 + N_0 W/P)^{1/2}}, & -2\pi W \leq \omega \leq 2\pi W, \\ 0, & \text{elsewhere.} \end{cases} \tag{40}$$

The bias term is obtained by using (38) in (17).

$$l_{B\infty} = -WT \ln\left(1 + \frac{P}{N_0 W}\right). \tag{41}$$

The resulting receiver is shown in Fig. 4.8. Notice that we cannot realize the filter in (40) exactly. We can approximate it arbitrarily closely by using an nth-order Butterworth filter, where n is chosen large enough to obtain the desired approximation accuracy.

To calculate the performance, we find $\mu_\infty(s)$ from (21). The result is

$$\mu_\infty(s) = \frac{T(1-s)}{N_0}\left\{N_0 W \ln\left(1 + \frac{P}{N_0 W}\right) - \frac{N_0 W}{(1-s)} \ln\left(1 + \frac{P(1-s)}{N_0 W}\right)\right\}. \tag{42}$$

This can be written as

$$\mu_\infty(s) = -\frac{2\bar{E}_r}{N_0} g_\infty(s, \Lambda_\infty), \tag{43}$$

where

$$\begin{aligned} g_\infty(s, \Lambda_\infty) &= -\frac{1}{2\Lambda_\infty}\left[(1-s)\ln(1 + \Lambda_\infty) - \ln(1 + (1-s)\Lambda_\infty)\right] \\ &= \frac{-1}{2\Lambda_\infty}\left[\ln\left[\frac{(1 + \Lambda_\infty)^{1-s}}{(1 + (1-s)\Lambda_\infty)}\right]\right] \end{aligned} \tag{44}$$

and

$$\Lambda_\infty = \frac{P}{N_0 W}. \tag{45}$$

Notice that the ∞ subscript of Λ_∞ and $g_\infty(\cdot, \cdot)$ denotes an infinite-order Butterworth spectrum. In Figs. 4.9 and 4.10, we plot the same results as in Example 1.

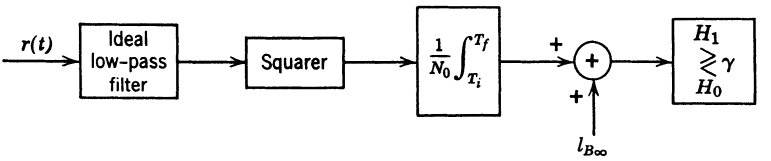

Fig. 4.8 Optimum receiver: ideal low-pass spectrum, long observation time.

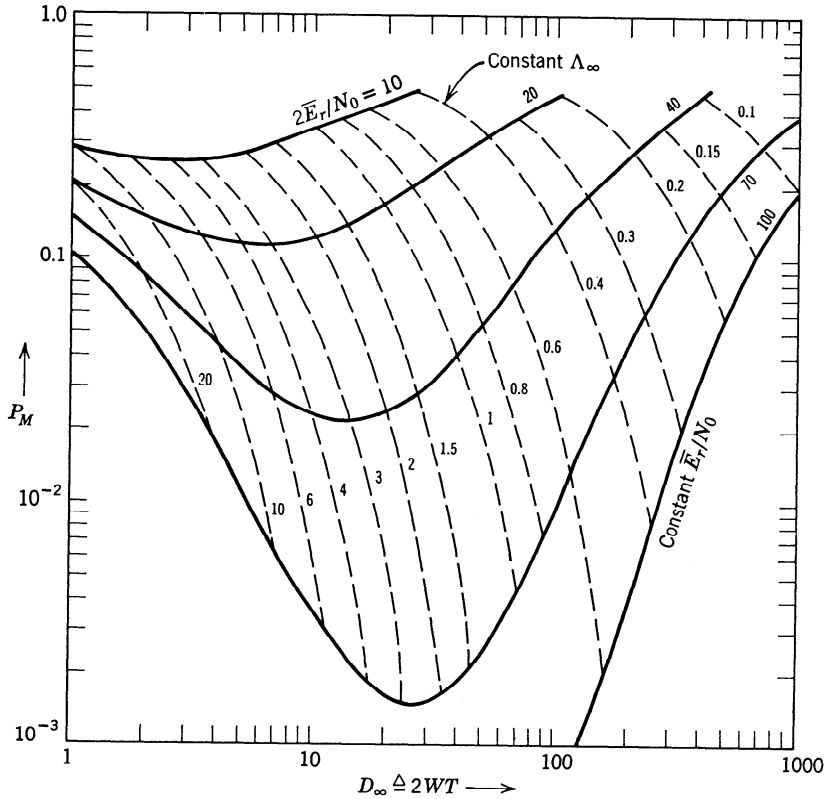

Fig. 4.9 Probability of miss versus time-bandwidth product, ideal bandlimited spectrum, $P_F = 10^{-1}$.

In this section we have considered the simple binary problem, developed the appropriate asymptotic formulas, and analyzed two typical examples. The next problem of interest is the general binary problem.

4.1.2 General Binary Problem

In Chapter 3 we extended the results from the simple binary case to the general binary case. Because of the strong similarities, we can simply summarize some of the appropriate asymptotic formulas for the general case. In Table 4.1, we have listed the transfer functions of the filters in the optimum receiver. In Table 4.2, we have listed the asymptotic formulas for $\mu_\infty(s)$. In Table 4.3, we have listed various relationships that are useful in general binary problems.

To illustrate the application of some of these results, we consider two examples.

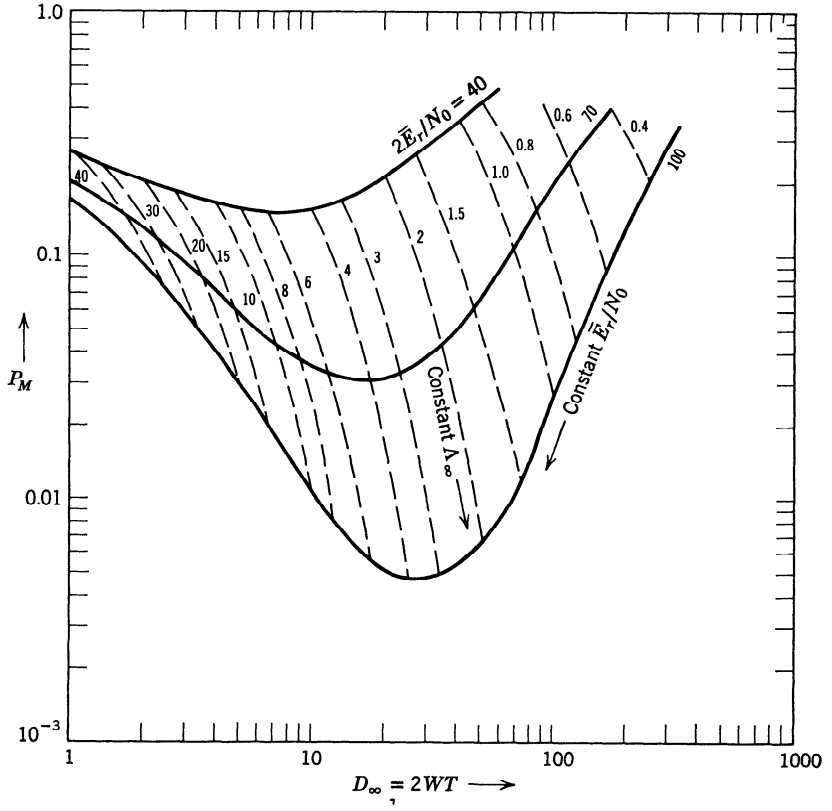

Fig. 4.10 Probability of miss versus time-bandwidth product, ideal bandlimited spectrum, $P_F = 10^{-3}$.

Example 3. In this example we consider a binary symmetric problem. The transmitted signals on the two hypotheses are

$$s_t(t) = \begin{cases} \sqrt{\dfrac{2E_t}{T}} \sin \omega_1 t, & T_i \leq t \leq T_f : H_1, \\ \sqrt{\dfrac{2E_t}{T}} \sin \omega_0 t, & T_i \leq t \leq T_f : H_0, \end{cases} \tag{46}$$

where

$$T \triangleq T_f - T_i. \tag{47}$$

The signal passes over a fluctuating Rayleigh channel.† The received waveforms are

$$\begin{aligned} r(t) &= s_1(t) + w(t), \qquad T_i \leq t \leq T_f : H_1, \\ r(t) &= s_0(t) + w(t), \qquad T_i \leq t \leq T_f : H_0. \end{aligned} \tag{48}$$

† We previously encountered fluctuating Rayleigh channels in Chapter II-8 and in the problem section of Chapter II-2. We discuss the model in more detail in Chapter 9.

Table 4.1 Asymptotic formulas for filters in optimum receivers

No.	Problem	Reference	SPLOT formula
1	General binary	(3.33)	$H_\Delta(j\omega) = \dfrac{S_{H_1}(\omega) - S_{H_0}(\omega)}{S_{H_1}(\omega)S_{H_0}(\omega)}$
2	Class A_w	(3.33)	$H_\Delta(j\omega) = \dfrac{S_{s_1}(\omega) - S_{s_0}(\omega)}{\left(S_{s_1}(\omega) + \dfrac{N_0}{2}\right)\left(S_{s_0}(\omega) + \dfrac{N_0}{2}\right)}$
3	Class B_w	(3.42)	$[H_\Delta(j\omega)]^+ = \left[\dfrac{S_s(\omega)}{(S_s(\omega) + S_n(\omega))S_n(\omega)}\right]^+$

Table 4.2 Asymptotic formulas for $\mu_\infty(s)$

No.	Problem	Reference	$\mu_\infty(s)$
1	General binary: nonsingular	(3.178)	$\mu_\infty(s) = T\displaystyle\int_{-\infty}^{\infty} \ln\left\{\frac{(S_{H_1}(\omega)/S_{H_0}(\omega))^{(s-1)/2}}{s + (1-s)[S_{H_1}(\omega)/S_{H_0}(\omega)]}\right\}\frac{d\omega}{2\pi}$
2	Class A_w	(3.60)	$\mu_\infty(s) = \dfrac{T}{2}\displaystyle\int_{-\infty}^{\infty}\left[(1-s)\ln\left(1 + \frac{2S_{s_1}(\omega)}{N_0}\right) + s\ln\left(1 + \frac{2S_{s_0}(\omega)}{N_0}\right) - \ln\left(1 + \frac{2(sS_{s_0}(\omega) + (1-s)S_{s_1}(\omega))}{N_0}\right)\right]\frac{d\omega}{2\pi}$
3	Class B	(3.60)	$\mu_\infty(s) = \dfrac{T}{2}\displaystyle\int_{-\infty}^{\infty}\ln\left\{\frac{[S_s(\omega) + S_n(\omega)]^{1-s}[S_n(\omega)]^s}{[(1-s)S_s(\omega) + S_n(\omega)]}\right\}\frac{d\omega}{2\pi}$
4	Class B_w	(3.60)	$\mu_\infty(s) = \dfrac{T}{2}\left\{(1-s)\displaystyle\int_{-\infty}^{\infty}\ln\left(1 + \frac{S_s(\omega)}{S_n(\omega) + (N_0/2)}\right)\frac{d\omega}{2\pi} - \int_{-\infty}^{\infty}\ln\left(1 + \frac{(1-s)S_s(\omega)}{S_n(\omega) + (N_0/2)}\right)\frac{d\omega}{2\pi}\right.$

Table 4.3 Relationship among various $\mu_\infty(s)$ results

No.	Reference	Relation
1	(3.101)	$\mu_{\mathrm{BP},\infty}(s) = 2\mu_{\mathrm{LP},\infty}(s)$
2	(3.65)	$\mu_{\mathrm{BS},\infty}(s) = \mu_{\mathrm{SIB},\infty}(s) + \mu_{\mathrm{SIB},\infty}(1-s)$
3	(3.73)	$\mu_{\mathrm{BS,BP},\infty}(\frac{1}{2}) = 4\mu_{\mathrm{SIB,LP},\infty}(\frac{1}{2})$

We assume that $s_0(t)$ and $s_1(t)$ are bandpass processes centered at ω_0 and ω_1, respectively, which are essentially disjoint and are symmetric about their respective carriers (see Figs. 3.7 and 3.8). The low-pass spectrum of the signal processes is $S_{s,\mathrm{LP}}(\omega)$, where

$$S_{s,\mathrm{LP}}(\omega) = \frac{2kP_{\mathrm{LP}}}{\omega^2 + k^2}. \tag{49}$$

The power in the received process depends on the transmitted power and the channel attenuation,

$$P_{\mathrm{LP}} \triangleq \frac{E_t\sigma_b^2}{T}, \tag{50}$$

where σ_b^2 is a measure of the mean-square channel strength. Notice that the total average received power is

$$P_r = 2P_{\mathrm{LP}}, \tag{51}$$

and that the total average received signal energy is

$$\bar{E}_r = 2\bar{E}_{r,\mathrm{LP}} = 2E_t\sigma_b^2 = 2P_{\mathrm{L}}\ T\sigma_b^2. \tag{52}$$

We assume that the hypotheses are equally likely and that the criterion is minimum Pr (ϵ).

The receiver structure follows easily by combining the results from the bandpass discussion (pages 74–77) with the results in Example 1 (page 104). The receiver is shown in Fig. 4.11. The four low-pass filters are identical:

$$H_{fr} = \frac{k\sqrt{1+\Lambda_1}}{j\omega + k\sqrt{1+\Lambda_1}}. \tag{53}$$

We have eliminated the ideal low-pass filters included in Fig. 3.9 because $H_{fr}(j\omega)$ is low-pass. We have also eliminated the gain in the integrator because it is the same in each path and the threshold is zero.

We can evaluate the performance by suitably modifying the results of Example 1. The first step to go from the low-pass asymmetric problem to the bandpass asymmetric problem. Recall from Table 4.3 that

$$\mu_{\mathrm{BP},\infty}(s) = 2\mu_{\mathrm{LP},\infty}(s). \tag{54}$$

Using (30) in (54) gives

$$\mu_{\mathrm{BP},\infty}(s) = \frac{2\bar{E}_r(1-s)}{N_0}\left\{\frac{1}{1+\sqrt{1+\Lambda_1}} - \frac{1}{1+\sqrt{1+(1-s)\Lambda_1}}\right\}, \tag{55}$$

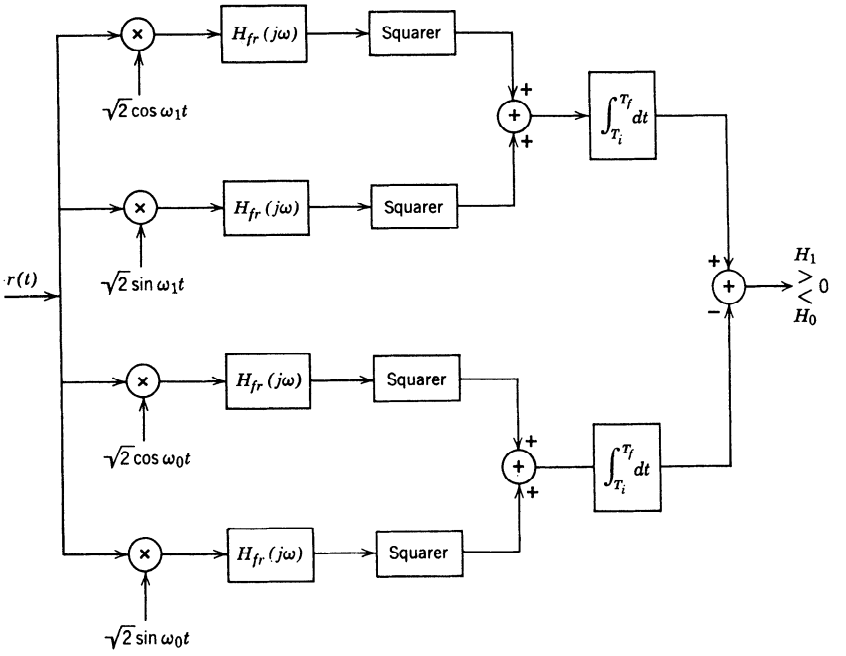

Fig. 4.11 Optimum receiver, binary symmetric bandpass problem, long observation time.

where

$$\Lambda_1 \triangleq \frac{4P_{\mathrm{LP}}}{kN_0}. \tag{56}$$

The next step is go from the asymmetric (or simple binary) problem to the binary symmetric problem. We recall that

$$\mu_{\mathrm{BS}}(s) = \mu_{\mathrm{SIB}}(s) + \mu_{\mathrm{SIB}}(1-s). \tag{57}$$

Using (55) in (57) gives

$$\mu_{\mathrm{BS,BP},\infty}(s) = \frac{2\bar{E}_r}{N_0}\left\{\frac{1}{1+\sqrt{1+\Lambda_1}} - \frac{(1-s)}{1+\sqrt{1+(1-s)\Lambda_1}} - \frac{s}{1+\sqrt{1+s\Lambda_1}}\right\}. \tag{58}$$

This reduces to

$$\mu_{\mathrm{BS,BP},\infty}(s) = \frac{2\bar{E}_r}{N_0}\left\{\frac{1}{\Lambda_1}[(1+\Lambda_1)^{1/2} - (1+\Lambda_1(1-s))^{1/2} - (1+\Lambda_1 s)^{1/2} + 1]\right\}. \tag{59}$$

The important quantity in the probability of error expressions is $\mu_{\mathrm{BS,BP},\infty}(\frac{1}{2})$ Letting $s = \frac{1}{2}$ in (59) gives

$$\mu_{\mathrm{BS,BP},\infty}(\tfrac{1}{2}) = \frac{2\bar{E}_r}{N_0}\left\{\frac{1}{\Lambda_1}\left[(1+\Lambda_1)^{1/2} - 2\left(1+\frac{\Lambda_1}{2}\right)^{1/2} + 1\right]\right\}. \tag{60}$$

If we define

$$g_{\mathrm{BP},1}(\Lambda_1) \triangleq \frac{-1}{2\Lambda_1}\left\{(1+\Lambda_1)^{1/2} - 2\left(1+\frac{\Lambda_1}{2}\right)^{1/2} + 1\right\}, \tag{61}$$

then we can write

$$\mu_{\mathrm{BS,BP},\infty}(\tfrac{1}{2}) = -\frac{\bar{E}_r}{N_0}\cdot 4g_{\mathrm{BP},1}(\Lambda_1). \tag{62}$$

We refer to $4g_{\mathrm{BP},1}(\Lambda_1)$ as the efficiency function of the binary communication system.

To find the approximate Pr (ϵ) we need $\ddot{\mu}_{\mathrm{BS,BP},\infty}(\frac{1}{2})$. Differentiating (59) twice with respect to s and evaluating the result at $s = \frac{1}{2}$, we have

$$\ddot{\mu}_{\mathrm{BS,BP},\infty}(\tfrac{1}{2}) = \frac{2\bar{E}_r}{N_0}\left\{\frac{\Lambda_1}{2}\left(1+\frac{\Lambda_1}{2}\right)^{-3/2}\right\}. \tag{63}$$

The approximate Pr (ϵ) follows from (3.77) as

$$\Pr(\epsilon) \simeq 2\left(\frac{N_0}{2\bar{E}_r}\right)^{1/2} \frac{[1+(\Lambda_1/2)]^{3/4}}{\sqrt{\pi\Lambda_1}} \exp\left[-4g_{\mathrm{BP},1}(\Lambda_1)\cdot\frac{\bar{E}_r}{N_0}\right]. \tag{64}$$

We see that the Pr (ϵ) depends on Λ_1, the signal-to-noise ratio in the signal process bandwidth, and $2\bar{E}_r/N_0$, the ratio of the average received signal energy to the noise spectral height.

The next step in the analysis depends on the transmitter constraints. If it is completely specified, we simply evaluate Pr (ϵ). If the signals are specified to be a segment of sine waves, as in (46), and the transmitter is peak-power-limited (i.e., E_t/T is limited), the performance is monotonic with T. On the other hand, if the transmitter is energy-limited, we may be able to optimize the performance by choosing T appropriately. This is an elementary version of the signal design problem. Later we shall look at the effect of different signal shapes.

We assume that σ_b^2, N_0, and k are fixed. Then, if we fix E_t, this fixes $\bar{E}_r$. The only remaining parameter is T (or, equivalently, Λ_1). We could choose Λ_1 to minimize the Pr (ϵ). A slightly easier procedure is to choose it to minimize $\mu_{\mathrm{BS,BP},\infty}(\frac{1}{2})$. From (60), we see that this is equivalent to maximizing the efficiency factor. In Fig. 4.12 we have plotted $g_{\mathrm{BP},1}(\Lambda_1)$ as a function of Λ_1. We see that the maximum occurs in the vicinity of $\Lambda_1 = 7$. We refer to this point as $\Lambda_{1,\mathrm{OPT}}$,

$$\Lambda_{1,\mathrm{OPT}} = 6.88, \tag{65}$$

and

$$g_{\mathrm{BP},1}(\Lambda_{1,\mathrm{OPT}}) = 0.0592. \tag{66}$$

We observe that the curve is very flat near the maximum, so that a precise adjustment of Λ_1 is not necessary. Using (66) in (64) gives an expression for the probability of error when the optimum value of Λ_1 is used.

$$\Pr_o(\epsilon) \simeq 1.32\left(\frac{N_0}{2\bar{E}_r}\right)\exp\left(-0.118\,\frac{\bar{E}_r}{N_0}\right). \tag{67}$$

We see that when the system uses the optimum value of Λ_1, the probability of error decreases exponentially with increasing $\bar{E}_r/N_0$.

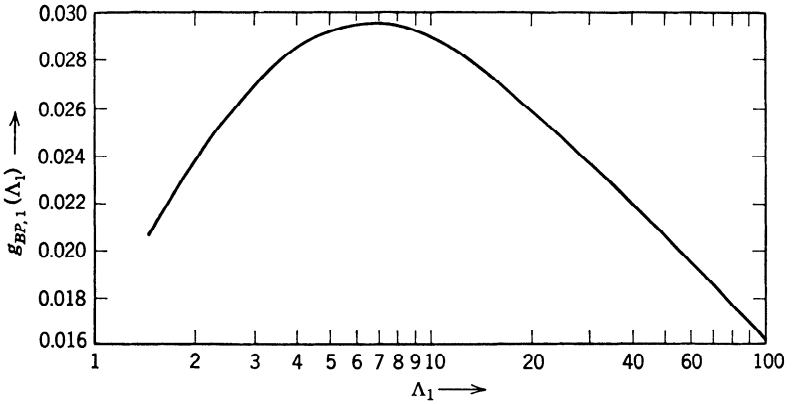

Fig. 4.12 $g_{\mathrm{BP},1}(\Lambda_1)$ **versus** Λ_1.

We now consider another example. All of the techniques are identical with Example 3. The reason for including the example is to derive some specific numerical results that we shall use later.

Example 4. Symmetric Hypotheses, Bandlimited Spectrum. The basic model is the same as in the preceding example [see (46) and (48)]. Now we assume that the low-pass signal process has a bandlimited spectrum

$$S_s(\omega) = \begin{cases} \dfrac{P_{\mathrm{LP}}}{2W}, & -2\pi W \leq \omega \leq 2\pi W, \\ 0, & \text{elsewhere.} \end{cases} \tag{68}$$

The receiver structure is an obvious combination of the structures in Figs. 4.8 and 4.11. As pointed out on page 109, we cannot realize the filters exactly but can approximate them arbitrarily closely. For the present we are concerned with the system performance. Using (42)–(45), Tables 4.2 and 4.3, and (68), we obtain

$$\mu_{\mathrm{BS,BP},\infty}(s) = -\frac{2\bar{E}_r}{N_0}\left\{\frac{1}{2\Lambda_\infty}\ln\left[\frac{[1+(1-s)\Lambda_\infty][1+s\Lambda_\infty]}{[1+\Lambda_\infty]}\right]\right\}, \tag{69}$$

where

$$\Lambda_\infty \triangleq \frac{P_{\mathrm{LP}}}{N_0 W}. \tag{70}$$

Letting $s = \frac{1}{2}$ in (69) gives

$$\mu_{\mathrm{BS,BP},\infty}(\tfrac{1}{2}) = -\frac{\bar{E}_r}{N_0}\cdot g_{\mathrm{BP},\infty}(\Lambda_\infty), \tag{71}$$

where we have defined

$$g_{\mathrm{BP},\infty}(\Lambda_\infty) \triangleq \frac{1}{\Lambda_\infty}\ln\left[\frac{[1+(\Lambda_\infty/2)]^2}{(1+\Lambda_\infty)}\right]. \tag{72}$$

Thus,

$$\exp\left[\mu_{\mathrm{BS,BP},\infty}(\tfrac{1}{2})\right] = \left\{\frac{[1 + (\Lambda_\infty/2)]^2}{(1 + \Lambda_\infty)}\right\}^{-\bar{E}_r/N_0\Lambda_\infty} \tag{73}$$

To get the coefficient for the approximate Pr (ϵ) expression, we differentiate (71) twice and evaluate the result at $s = \frac{1}{2}$. The result is

$$\ddot{\mu}_{\mathrm{BS,BP},\infty}(\tfrac{1}{2}) = \frac{2\bar{E}_r}{N_0}\frac{\Lambda_\infty}{[1 + (\Lambda_\infty/2)]^2}. \tag{74}$$

Then, using (3.76),

$$\Pr(\epsilon) \simeq \frac{(1 + \Lambda_\infty)^{WT}}{\sqrt{\pi WT}\,\Lambda_\infty[1 + (\Lambda_\infty/2)]^{2WT-1}} \tag{75}$$

As before, we can find an optimum value of Λ_∞ by maximizing $g_{\mathrm{BP},\infty}(\Lambda_\infty)$. The result is

$$\Lambda_{\infty,\mathrm{OPT}} = \frac{\bar{E}_r/N_0}{2WT} = 3.07. \tag{76}$$

Substituting (76) into (75), we obtain

$$\Pr_0(\epsilon) \simeq \sqrt{\frac{0.815}{\bar{E}_r/N_0}}\exp\left(-0.1488\left[\frac{\bar{E}_r}{N_0}\right]\right). \tag{77}$$

We see that the magnitude of the coefficient in the exponent of (77) is slightly larger than in the one-pole case [recall (67)].

The communication systems in Examples 3 and 4 have illustrated the application of long-time approximations to particular problems. In addition, they have given us some interesting results for binary FSK communication over fluctuating symmetric Rayleigh channels. It is interesting to compare these results with those we obtained in Chapter I-4 for binary PSK and FSK systems operating over an additive noise channel. From (I-4.40) and (I-4.36) we have

$$\Pr_{\mathrm{FSK}}(\epsilon) = \mathrm{erfc}_*\left(\sqrt{\frac{E_r}{N_0}}\right), \tag{78}$$

or

$$\Pr_{\mathrm{FSK}}(\epsilon) \simeq \left(\frac{N_0}{2\pi E_r}\right)^{1/2}\exp\left(-\frac{E_r}{2N_0}\right), \qquad \sqrt{\frac{E_r}{N_0}} \geq 2. \tag{79}$$

Similarly,

$$\Pr_{\mathrm{PSK}}(\epsilon) \simeq \left(\frac{N_0}{\pi E_r}\right)^{1/2}\exp\left(-\frac{E_r}{N_0}\right), \qquad \sqrt{\frac{E_r}{N_0}} \geq 2. \tag{80}$$

Recall that the received signal energy is fixed in an additive noise channel. The results from (67), (77), (79), and (80) are summarized in Table 4.4.

Table 4.4 Efficiency Factors for Various Binary Communication Systems (Large $\bar{E}_r/N_0$)

System	Signals	Channel	Efficiency Factor	Loss in db (relative to system 1)
1	PSK	Additive white Gaussian noise	1.0	0
2	FSK	Additive white Gaussian noise	0.5	3
3	FSK	Rayleigh channel: ideal bandlimited spectrum	0.149	8.28
4	FSK	Rayleigh channel: one-pole spectrum	0.118	9.30

We denote the coefficient of $\bar{E}_r/N_0$ as the *efficiency factor* of a particular communication scheme. Comparing the exponents, we see that a bandlimited Rayleigh channel requires about 5.28 db more average energy than the binary FSK system to obtain the same error exponent. A Rayleigh channel with a first-order Butterworth spectrum requires about 6.30 db more average energy to obtain the same error exponent. We have assumed that $\bar{E}_r/N_0$ is large.

There are several restrictions to our analysis that should be emphasized:

1. We assumed that a rectangular pulse was transmitted. In Chapter 11, we shall prove that the efficiency factor for *any* Rayleigh channel and any signal shape is bounded by 0.1488. We shall see that for certain channels the system in Example 4 corresponds to the optimum binary orthogonal signaling scheme.

2. We used long-time-interval approximations. If $\bar{E}_r/N_0$ is large and we use the optimum time-bandwidth product, the approximation will always be valid.

3. We detected each signal individually and did not try to exploit the continuity of the channel from baud to baud by performing a continuous measurement. In Section 5.1.3, we shall discuss this type of system briefly.

4. We considered only Rayleigh channels whose fading spectra were symmetric about the carrier. In Chapter 11, we shall analyze more general channels.

We now summarize briefly the results for the long time interval–stationary process case.

4.1.3 Summary: SPLOT Problem

In this section we studied the case in which the received waveform is a sample function of a stationary random process *and* the observation interval is long. By neglecting the transient effects at the ends of the observation interval, we were able to implement the receiver using time-invariant filters. The resulting receiver is suboptimum but approaches the optimum receiver rapidly as the time-bandwidth product of the signal process increases.

We have not discussed how long the observation interval must be in order for the SPLOT approximation to be valid. Whenever the processes have rational spectra, we can compute the performance of both the optimum receiver and the SPLOT receiver using state-variable techniques. Thus, in any particular situation we can check the validity of the approximation quantitatively. A conservative requirement for using the approximation is to check the time-bandwidth product at the input to the squarer in Canonical Realization No. 3. If the product is greater than 5, the approximation is almost always valid. In many cases, the SPLOT receiver is essentially optimum for products as low as 2.

The performance expressions for the SPLOT case were simplified because we could use the asymptotic expressions for the Fredholm determinant. Thus, the calculation of $\mu_\infty(s)$ always reduced to finding the mean-square filtering error in some realizable Wiener filtering problem. This reduction meant that many of the detailed results in Section I-6.2 were directly applicable to the Gaussian detection problem. In many situations we can exploit this similarity to obtain answers efficiently.

In addition to considering the general SPLOT problem, we considered the problem of binary communication over a Rayleigh channel. We found that if we were allowed to control the time-bandwidth product of the receiver signal process, we could achieve a Pr (ϵ) that decreased exponentially with $\bar{E}_r/N_0$. This behavior was in contrast to the nonfluctuating Rayleigh channel discussed in Section I-4.4.2, in which the Pr (ϵ) decreased linearly with $\bar{E}_r/N_0$.

This completes our discussion of the SPLOT problem. There are a number of problems in Section 4.5 that illustrate the application of the results to specific situations.

4.2 SEPARABLE KERNELS

In this section we consider a class of signal covariance functions that lead to a straightforward solution for the optimum receiver and its

performance. In Section 4.2.1, we consider the separable kernel model and derive the necessary equations that specify the optimum receiver and its performance. In Sections 4.2.2 and 4.2.3, we consider physical situations in which the separable kernel model is valid. Finally, in Section 4.2.4, we summarize our results.

4.2.1 Separable Kernel Model

Our initial discussion is in the context of the simple binary problem with zero-mean processes. The received waveforms on the two hypotheses are

$$\begin{aligned} r(t) &= s(t) + w(t), \qquad T_i \leq t \leq T_f: H_1, \\ r(t) &= w(t), \qquad T_i \leq t \leq T_f: H_0. \end{aligned} \tag{81}$$

The noise $w(t)$ is a sample function from a zero-mean white Gaussian random process with spectral height $N_0/2$. The signal $s(t)$ is a sample function from a zero-mean Gaussian random process with covariance function $K_s(t, u)$.

From (2.28) the LRT is

$$l_R = \frac{1}{N_0} \int_{T_i}^{T_f} \int r(t) h_1(t, u) r(u)\, dt\, du \underset{H_0}{\overset{H_1}{\gtrless}} \gamma, \tag{82a}$$

where $h_1(t, u)$ is specified by the integral equation

$$\frac{N_0}{2} h_1(t, u) + \int_{T_i}^{T_f} h_1(t, z) K_s(z, u)\, dz = K_s(t, u), \qquad T_i \leq t, u \leq T_f. \tag{82b}$$

In Section I-4.3.6 we studied solution techniques for this integral equation. On page I-322, we observed that whenever the kernel of the integral equation [i.e., the signal covariance function $K_s(t, u)$] was separable, the solution to (82*b*) followed by inspection. A separable kernel corresponds to a signal process with a finite number of eigenvalues. Thus, we can write

$$\boxed{K_s(t, u) = \sum_{i=1}^{K} \lambda_i^s \phi_i(t) \phi_i(u), \qquad T_i \leq t, u \leq T_f,} \tag{83}$$

where $\phi_i(t)$ and λ_i^s are the eigenfunctions and eigenvalues, respectively, of the signal process. In this case the solution to (82*b*) is

$$h_1(t, u) = \sum_{i=1}^{K} h_i \phi_i(t) \phi_i(u) = \sum_{i=1}^{K} \frac{\lambda_i^s}{(N_0/2) + \lambda_i^s} \phi_i(t) \phi_i(u), \qquad T_i \leq t, u \leq T_f. \tag{84}$$

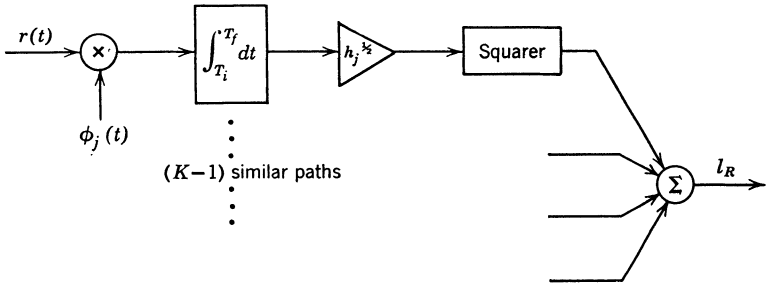

Fig. 4.13 Correlator realization of separable kernel receiver.

This can be verified by substituting (84) into (82*b*). For separable kernels, the simplest realization is Canonical Realization No. 3 (the filter-squarer receiver). From (2.45),

$$h_1(t, u) = \int_{T_i}^{T_f} h_f(z, t)h_f(z, u)\, dz, \tag{85}$$

whose solution is

$$h_{fu}(z, t) = \sum_{i=1}^{K} h_i^{1/2}\phi_i(z)\phi_i(t), \qquad T_i \leq t, z \leq T_f. \tag{86}$$

Using (85) and (86) in (82*a*) and performing the integration on z we obtain

$$\boxed{l_R = \frac{1}{N_0}\sum_{i=1}^{K} h_i\left[\int_{T_i}^{T_f} r(t)\phi_i(t)\, dt\right]^2}. \tag{87}$$

The operations on $r(t)$ can be realized using either correlators or matched filters. These realizations are shown in Figs. 4.13 and 4.14. These receiver structures are familiar from Fig. I-4.66 on page I-353. Looking at

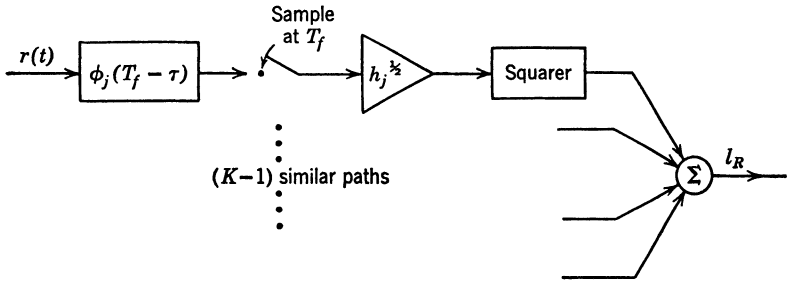

Fig. 4.14 Matched filter realization of separable kernel receiver.

(I-4.399), we see that the received signal on H_1 was

$$r(t) = \sum_{i=1}^{K} a_i s_i(t) + w(t), \qquad 0 \leq t \leq T, \tag{88}$$

where the a_i are $N(0, \sigma_{a_i})$ and the $s_i(t)$ are orthonormal. The total signal is

$$s(t) = \sum_{i=1}^{K} a_i s_i(t), \tag{89}$$

which is a zero-mean Gaussian process with covariance function

$$K_s(t, u) = \sum_{i=1}^{K} \sigma_{a_i}^2 s_i(t) s_i(u), \qquad 0 < t, u \leq T. \tag{90}$$

Comparing (90) and (83), we see that the separable kernel problem is identical with the problem that we solved in Section I-4.4.2, in the context of an unwanted parameter problem. As we observed on page I-353, the problem is also identical with the general Gaussian problem that we solved in Section I-2.6. The reason for this simplification is that the signal has only a finite number of eigenvalues. Thus, we can immediately map $r(t)$ into a K-dimensional vector $\mathbf{r}$ that is a sufficient statistic. Therefore, all of the examples in Sections I-2.6 and I-4.4 correspond to separable kernel Gaussian process problems, and we have a collection of results that are useful here.

The approximate performance of the optimum receiver is obtained by calculating $\mu(s)$ and using the approximate expressions in (2.166) and (2.174). From the first term in (2.132), we have

$$\boxed{\mu_R(s) = \tfrac{1}{2} \sum_{i=1}^{K} \ln \left\{ \frac{(1 + 2\lambda_i^s/N_0)^{1-s}}{1 + [2(1-s)/N_0]\lambda_i^s} \right\}.} \tag{91}$$

Using (91) in (2.166) and (2.174) gives an approximate expression for P_F and P_M. We recall that when the K eigenvalues were equal we could obtain an exact expression. Even in this case the approximate expressions are easier to use and give accurate answers for moderate K (see Fig. I-2.42).

At this point we have established that the separable kernel problem is identical with problems that we have already solved. The next step is to discuss several important physical situations in which the signal processes have separable kernels.

4.2.2 Time Diversity

Historically, the first place that this type of problem arose was in pulsed radar systems. The transmitted signal is a sequence of pulsed sinusoids

at a carrier frequency $\omega_c = 2n\pi/T$, where n is a large integer. The sequence is shown in Fig. 4.15. The ith signal is

$$s_i(t) \triangleq \begin{cases} \sqrt{\frac{2}{T}} \sin \omega_c t, & (i-1)T_p \leq t \leq (i-1)T_p + T, \\ 0, & \text{elsewhere.} \end{cases} \tag{92}$$

If a target is present, the pulses are reflected. We shall discuss target reflection models in detail in Chapter 9. There we shall see that for many targets the reflection from the ith pulse can be modeled as

$$s_{ri}(t) = \begin{cases} v_i \sqrt{\frac{2}{T}} \sin(\omega_c t + \phi_i), & (i-1)T_p \leq t \leq (i-1)T_p + T, \\ 0, & \text{elsewhere,} \end{cases} \tag{93}$$

where the v_i are Rayleigh random variables and the ϕ_i are uniform random variables. (Notice that we have put the target at zero range for simplicity.) As in Section I-4.4.2, we write $s_{ri}(t)$ in terms of two quadrature components,

$$s_{ri}(t) \triangleq \begin{cases} b_{si} \sqrt{\frac{2}{T}} \sin \omega_c t + b_{ci} \sqrt{\frac{2}{T}} \cos \omega_c t, \\ \qquad\qquad (i-1)T_p \leq t \leq (i-1)T_p + T, \\ 0, \quad \text{elsewhere.} \end{cases} \tag{94a}$$

Equivalently, we can write

$$s_{ri}(t) \triangleq b_{si}\phi_{si}(t) + b_{ci}\phi_{ci}(t), \qquad -\infty < t < \infty, \tag{94b}$$

where $\phi_{si}(t)$ and $\phi_{ci}(t)$ include the time interval in their definition. The b_{si} and b_{ci} are statistically independent Gaussian random variables with variances σ_b^2. The average received energy per pulse is

$$\bar{E}_{r1} \triangleq 2\sigma_b^2. \tag{95}$$

The received waveform consists of the signal reflected from the sequence of pulses plus a white noise component,

$$r(t) = \sum_{i=1}^{K} [b_{si}\phi_{si}(t) + b_{ci}\phi_{ci}(t)] + w(t), \qquad T_i \leq t \leq T_f. \tag{96}$$

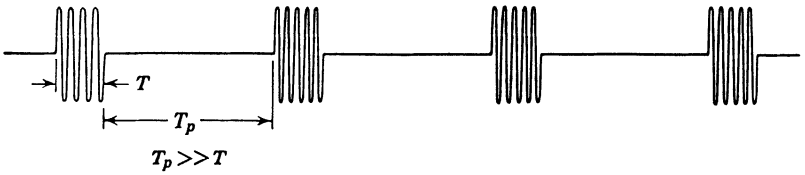

Fig. 4.15 Transmitted pulse sequence.

The observation interval includes all of the reflected pulses completely. Now, when we let v_i and ϕ_i be random variables, we are assuming that the target reflection is essentially constant over the pulse duration. In general, T_p is much larger than the pulse duration. Thus, if the target is fluctuating, it is plausible to assume that the v_i and ϕ_i are independent random variables for different i. This means that the b_{ci} and b_{si} are independent for different i. The covariance function of the signal process is

$$K_s(t, u) = \sum_{i=1}^{K} \{\sigma_b^2 \phi_{ci}(t)\phi_{ci}(u) + \sigma_b^2 \phi_{si}(t)\phi_{si}(u)\}, \qquad T_i \leq t, u \leq T_f. \tag{97}$$

Thus we have a separable kernel with $2K$ equal eigenvalues. Using Figs. 4.13 and I-4.68, we obtain the receiver structure shown in Fig. 4.16. Here the orthogonality arises because the signals are nonoverlapping in time. We refer to this as the time-diversity case.

We have already computed the performance for this problem (Case 1A on page I-108). By letting

$$N = 2K, \tag{98}$$

$$\sigma_s^2 = \sigma_b^2 = \frac{\bar{E}_{r1}}{2}, \tag{99}$$

$$\sigma_n^2 = \frac{N_0}{2}, \tag{100}$$

the results in Fig. I-2.35 apply directly. Notice that

$$\mu_{\mathrm{BP,SK}}(s) = K \ln \left[\frac{(1 + \bar{E}_{r1}/N_0)^{1-s}}{1 + (1 - s)(\bar{E}_{r1}/N_0)} \right] \tag{101}$$

[use either (I-2.501) or (91)].

The ROC is shown in Fig. 4.17. The average received signal energy per pulse is $\bar{E}_{r1}$, and the total average received energy is $\bar{E}_r$, where

$$\bar{E}_r = K\bar{E}_{r1}. \tag{102}$$

In Fig. 4.18, we fix $\bar{E}_r$ and P_F and plot P_M as a function of K. (These are Figs. I-2.35*b* and *c* relabeled.) This shows us how to optimize the number

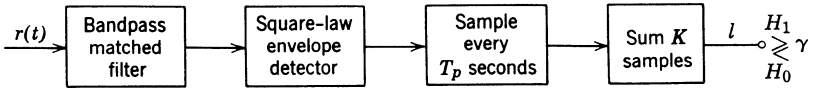

Fig. 4.16 Optimum receiver for pulsed radar problem.

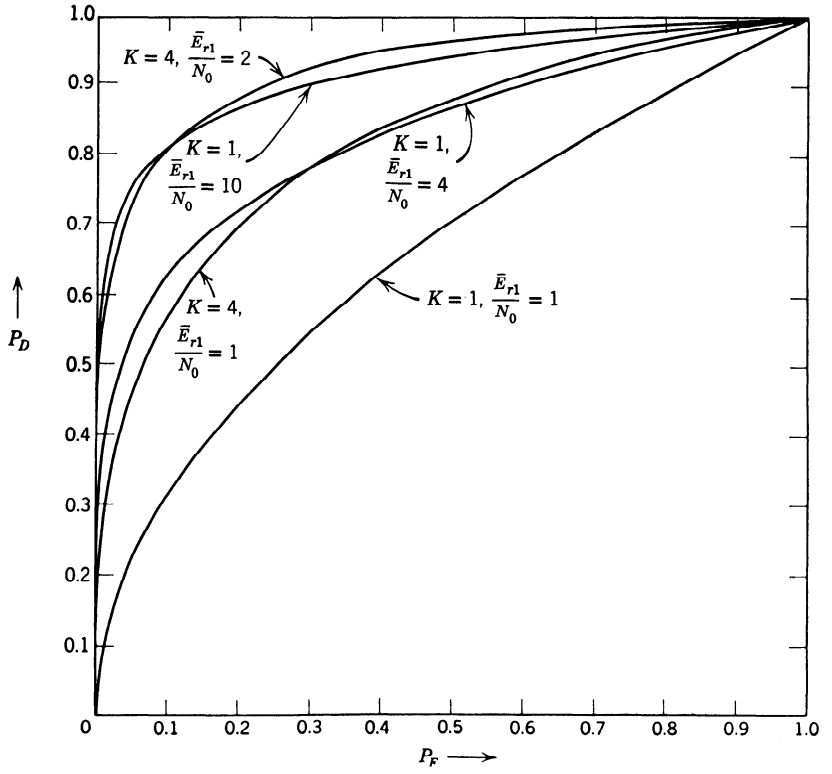

Fig. 4.17 Receiver operating characteristic: pulsed radar, Rayleigh target.

of transmitted pulses in various situations. Notice that Fig. I-2.35 was based on an exact calculation. As shown in Fig. I-2.42, an approximate calculation gives a similar results.

A second place that time-diversity occurs is in ionospheric communication. In the HF frequency range, long-range communication schemes frequently rely on waves reflected from the ionosphere. As a result of multiple paths, a single transmitted pulse may cause a sequence of pulses to appear at the receiver. Having traveled by separate paths, the amplitudes and phases of the different pulses are usually not related. A typical situation is shown in Fig. 4.19. If the output pulses do not overlap, this is commonly referred to as a resolvable multipath problem. If the path lengths are known (we discuss the problem of unknown path lengths in a later section), this is identical with the time diversity problem above.

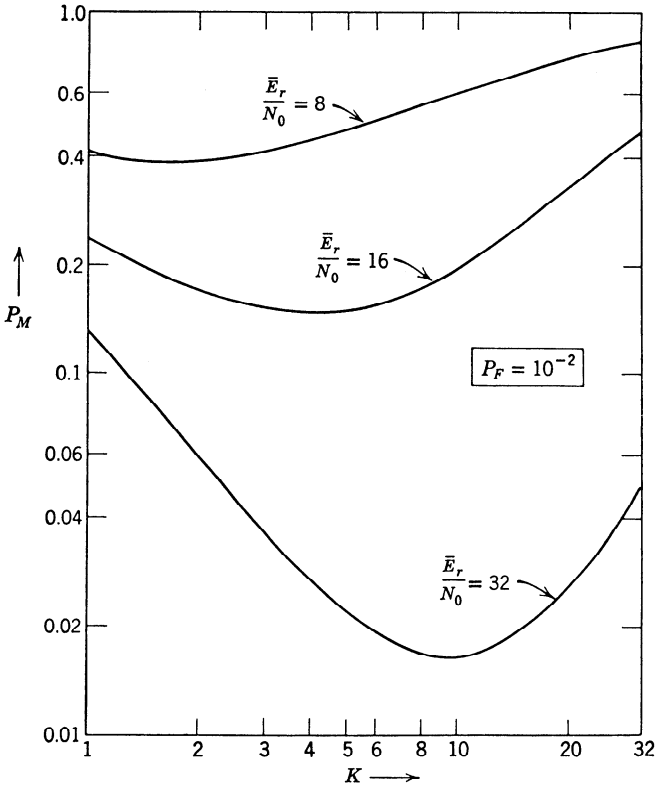

Fig. 4.18 P_M **as a function of the number of transmitted pulses (total energy fixed).**

4.2.3 Frequency Diversity

The obvious dual to the time problem occurs when we transmit K pulses at different frequencies but at the same time. A typical application would be a frequency diversity communication system operating over K nonfluctuating Rayleigh channels. On H_1, we transmit K signals in disjoint frequency bands,

$$s_{t1}(t) = \begin{cases} \sum_{i=1}^{K} \sqrt{\frac{2}{T}} \sin \omega_{1i} t, & 0 \leq t \leq T, \\ 0, & \text{elsewhere.} \end{cases} \tag{103}$$

On H_0, we transmit K signals in a different set of disjoint frequency bands,

$$s_{t0}(t) = \begin{cases} \sum_{j=1}^{K} \sqrt{\frac{2}{T}} \sin \omega_{0j} t, & 0 \leq t \leq T, \\ 0, & \text{elsewhere.} \end{cases} \tag{104}$$

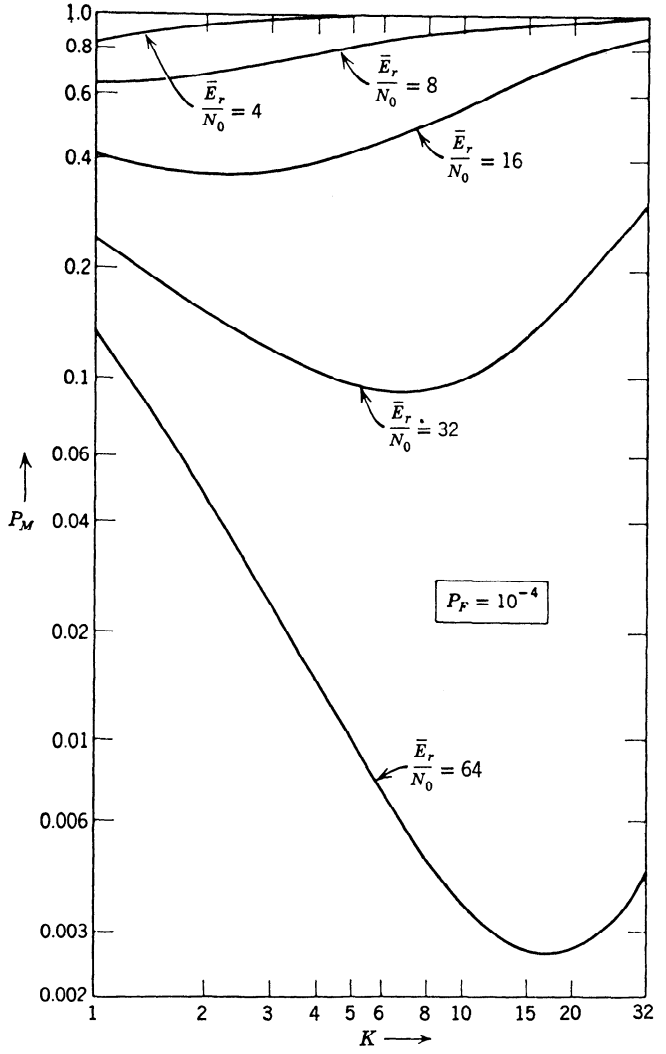

Fig. 4.18 (Continued.)

Each of the K transmitted signals passes over a Rayleigh channel. The output is

$$\begin{aligned} r(t) &= \sum_{i=1}^{K} v_i \sqrt{\frac{2}{T}} \sin [\omega_{1i} t + \phi_i] + w(t), \qquad 0 \leq t \leq T : H_1, \\ r(t) &= \sum_{j=1}^{K} v_j \sqrt{\frac{2}{T}} \sin [\omega_{0j} t + \phi_j] + w(t), \qquad 0 \leq t \leq T : H_0. \end{aligned} \tag{105}$$

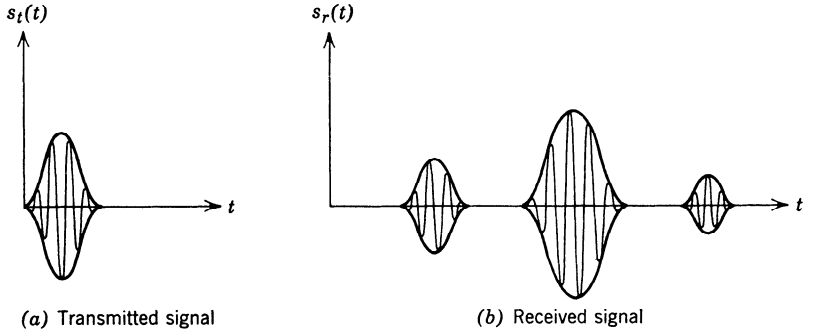

(a) Transmitted signal (b) Received signal

Fig. 4.19 Ionospheric model: resolvable multipath.

The frequencies ω_{1i} and ω_{0j} are chosen so that the outputs due to the signals are orthogonal. We shall assume that the fading in the different Rayleigh channels is statistically independent and that each channel has identical statistical characteristics. The average received signal energy in each channel is

$$E(v_i^2) = 2\sigma_b^2 \triangleq \bar{E}_{r_i}. \tag{106}$$

We see that this problem is just the binary symmetric version of the problem in Section 4.2.2. The optimum receiver structure is shown in Fig. 4.20. To evaluate the performance, we observe that this case is mathematically identical with Example 3A on pages I-130–I-132 if we let

$$N = 2K, \tag{107}$$

$$\sigma_s^2 = \sigma_b^2 = \frac{\bar{E}_{r1}}{2}, \tag{108}$$

and

$$\sigma_n^2 = \frac{N_0}{2}. \tag{109}$$

Then $\mu(\frac{1}{2})$ is given by (I-2.510) as

$$\boxed{\mu_{\text{BS, BP, SK}}(\tfrac{1}{2}) = K \ln \left\{ \frac{1 + \bar{E}_{r1}/N_0}{(1 + \bar{E}_{r1}/2N_0)^2} \right\}.} \tag{110}$$

We can also obtain (110) by using Table 4.3 and (101). A bound on the Pr (ϵ) follows from (I-2.473) and (110) as

$$\Pr(\epsilon) \leq \frac{1}{2} \left\{ \frac{(1 + \bar{E}_{r1}/N_0)}{(1 + \bar{E}_{r1}/2N_0)^2} \right\}^K. \tag{111}$$

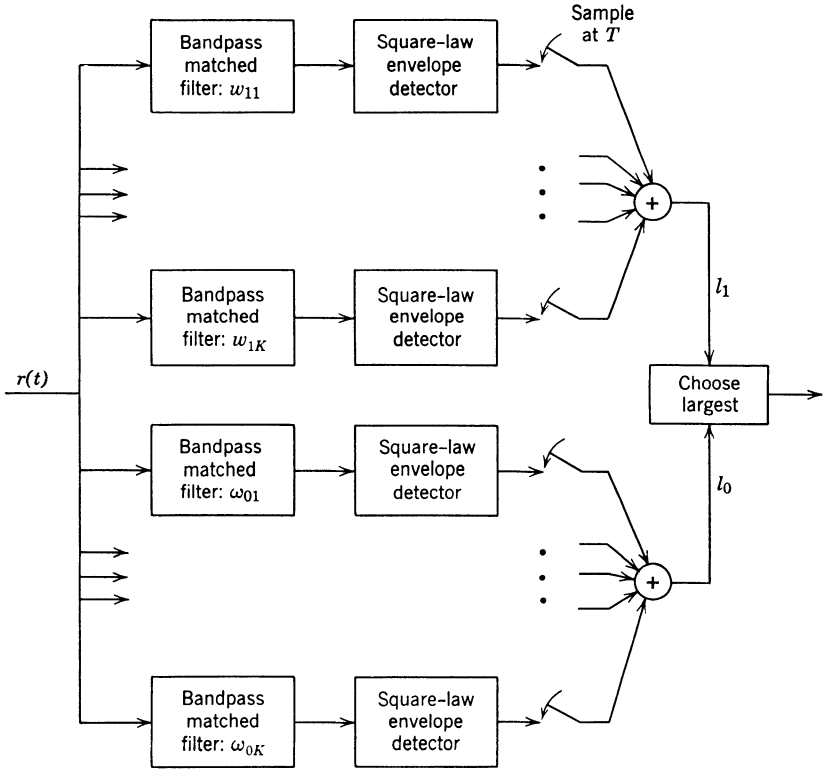

Fig. 4.20 Frequency diversity receiver.

An approximate error expression is given by (I-2.516) and (110) as

$$\Pr(\epsilon) \simeq \sqrt{\frac{1}{\pi K}} \frac{(1 + \bar{E}_{r1}/N_0)^K}{(\bar{E}_{r1}/N_0)(1 + \bar{E}_{r1}/2N_0)^{K/2-1}}. \tag{112}$$

Frequently the total energy available at the transmitter is fixed. We want to divide it among the various diversity branches in order to minimize the Pr (ϵ). When the channel attenuations are equal, the optimum division can be calculated easily using either exact or approximate Pr (ϵ) expressions. The simplest procedure is to introduce an efficiency factor for the diversity system.

$$\mu_{\mathrm{BS,BP,SK}}(\tfrac{1}{2}) = -\frac{\bar{E}_r}{N_0} g_d(\lambda), \tag{113}$$

where

$$g_d(\lambda) = \frac{1}{\lambda} \ln \left\{ \frac{(1 + \lambda/2)^2}{(1 + \lambda)} \right\} \tag{114}$$

and

$$\lambda = \frac{\bar{E}_{r1}}{N_0}. \tag{115}$$

We see that $g_d(\lambda)$ is identical with $g_{BP,\infty}(\Lambda_\infty)$ in Example 4 on page 116. Thus, it is maximized by choosing

$$\lambda_{\text{OPT}} = \left(\frac{\bar{E}_{r1}}{N_0} \right)_{\text{OPT}} = 3.07, \tag{116}$$

and the Pr (ϵ) is given by (78). The result in (116) says that the optimum strategy is to divide the energy so that the average energy-to-noise spectral height ratio in each Rayleigh channel is 3.07.

The comparison of these two results is interesting. In this case we optimized the performance by choosing the diversity properly. Previously we chose the signal-to-noise ratio in the signal process bandwidth properly. The relationship between the two problems is clear if we interpret both problems in terms of eigenvalues. In the case of the bandlimited spectrum, there are $4WT$ equal eigenvalues (for $WT \gg 1$) and in the diversity system there are $2K$ equal eigenvalues.

4.2.4 Summary: Separable Kernels

In this section we have studied the separable kernel problem. Here, the receiver output consists of a weighted sum of the squares of a finite number of statistically independent Gaussian variables. The important difference between the separable kernel case and the general Gaussian problem is that we have *finite* sums rather than *infinite* sums. Therefore, in principle at least, we can always calculate the performance exactly. As we observed in Chapter I-2, if the eigenvalues are different and K is large, the procedure is tedious. If the eigenvalues are equal, the sufficient statistic has a chi-squared density (see page I-109). This leads to an exact expression for P_F and P_D. As discussed in Section I-2.7 (page I-128), our approximate expressions based on $\mu(s)$ are accurate for moderate K. Thus, even in cases when an exact probability density is available, we shall normally use the approximate expressions because of their simplicity.

In the foregoing text we have considered examples in which the signal process had equal eigenvalues and the additive noise was white. In the problems in Section 4.5, we consider more general separable kernel problems.

4.3 LOW-ENERGY-COHERENCE (LEC) CASE†

In this section we consider the simple binary problem described in Chapter 2 (page 8). The received waveforms on the two hypotheses are

$$\begin{aligned} r(t) &= s(t) + w(t), \qquad T_i \leq t \leq T_f: H_1, \\ r(t) &= w(t), \qquad\quad T_i \leq t \leq T_f: H_0. \end{aligned} \tag{117}$$

We assume that $w(t)$ is a white, zero-mean Gaussian process with spectral height $N_0/2$ and that $s(t)$ is a zero-mean Gaussian random process with covariance function $K_s(t, u)$. The signal covariance function can be written as a series,

$$K_s(t, u) = \sum_{i=1}^{\infty} \lambda_i^s \phi_i(t)\phi_i(u), \qquad T_i \leq t, u \leq T_f. \tag{118}$$

If we write $s(t)$ in a Karhunen-Loève expansion, the eigenvalue, λ_i^s, is the mean-square value of the ith coefficient. Physically this corresponds to the average energy along each eigenfunction. If all of the signal energy were contained in a single eigenvalue, we could write

$$s(t) = s_1\phi_1(t) \tag{119}$$

and the problem would reduce to known signal with Gaussian random amplitude that we solved in Section I-4.4. This problem is sometimes referred to as a *coherent* detection problem because all of the energy is along a single known signal.

In many physical situations we have a completely different behavior. Specifically, when we write

$$s(t) = \sum_{i=1}^{\infty} s_i\phi_i(t), \qquad T_i \leq t \leq T_f, \tag{120}$$

we find that the energy is distributed along a large number of coordinates and that all of the eigenvalues are small compared to the white noise level. Specifically,

$$\lambda_i^s \ll \frac{N_0}{2}, \qquad i = 1, 2, \ldots. \tag{121}$$

We refer to this case as the *low-energy-coherence* (LEC) case. In this section we study the implications of the restriction in (121) with respect

† Most of the original work in the low-energy-coherence case is due to Price [1], [2] and Middleton [3], [5], [7]. It is sometimes referred to as the "coherently undetectable" or "threshold" case. Approaching the performance through $\mu(s)$ is new, but it leads to the same results as obtained in the above references. In [9], Middleton discusses the threshold problem from a different viewpoint. Other references include [10], [11].

to the optimum receiver structure and its performance. Before we begin our discussion, several observations are worthwhile.

1. When $s(t)$ is a stationary process, we know from page I-208 that

$$\lambda_i^s \leq \lambda_{\max} \leq \max_f S_s(f). \tag{122}$$

Thus, if

$$\max_f S_s(f) \ll \frac{N_0}{2}, \tag{123}$$

the LEC condition exists.

2. It might appear that the LEC condition implies poor detection performance and is therefore uninteresting. This is not true, because the receiver output is obtained by combining a large number of components. Even though each signal eigenvalue is small, the resulting test statistic may have appreciably different probability densities on the two hypotheses.

3. We shall find that the LEC condition leads to appreciably simpler receiver configurations and performance calculations. Later we shall examine the effect of using these simpler receivers when the LEC condition is not satisfied.

We begin our discussion with the general results obtained in Section 2.1. From (2.31) we have

$$l_R = \frac{1}{N_0} \int_{T_i}^{T_f} \int r(t) h_1(t, u) r(u)\, dt\, du, \tag{124}$$

and from (2.19),

$$l_R = \frac{1}{2}\left(\frac{2}{N_0}\right)^2 \sum_{i=1}^{\infty} \left(\frac{\lambda_i^s}{1 + (2/N_0)\lambda_i^s}\right) r_i^2. \tag{125}$$

To get an approximate expression, we denote the largest eigenvalue by $\lambda_{\max}^s$. If

$$\lambda_{\max}^s < \frac{N_0}{2}, \tag{126}$$

we can expand each term of the sum in (125) in a power series in λ_i,

$$l_R = \frac{1}{2}\left(\frac{2}{N_0}\right)^2 \sum_{i=1}^{\infty} \lambda_i^s \left[1 - \frac{2}{N_0}\lambda_i^s + \left(\frac{2}{N_0}\right)^2 (\lambda_i^s)^2 - \cdots\right] r_i^2. \tag{127}$$

The convergence of each expansion is guaranteed by the condition in (126). The LEC condition in (121) is more stringent that (126). When

$$\boxed{\frac{2}{N_0}\lambda_{\max}^s \ll 1, \qquad \text{[LEC condition]}} \tag{128}$$

we can approximate l_R by retaining the first *two* terms in the series. The reason for retaining two terms is that they are of the order in $2\lambda_i^s/N_0$. (The reader should verify this.) The first term is

$$l_R^{(1)} = \frac{1}{2}\left(\frac{2}{N_0}\right)^2 \sum_{i=1}^{\infty} \lambda_i^s r_i^2 = \frac{1}{2}\left(\frac{2}{N_0}\right)^2 \int_{T_i}^{T_f}\int r(t)K_s(t, u)r(u)\, dt\, du. \tag{129}$$

The second term is

$$l_R^{(2)} = -\frac{1}{2}\left(\frac{2}{N_0}\right)^3 \sum_{i=1}^{\infty} (\lambda_i^s)^2 r_i^2. \tag{130}$$

If we define a kernel

$$\begin{aligned} K_s^{(2)}(t, u) &= \int_{T_i}^{T_f} K_s(t, z)K_s(u, z)\, dz \\ &= \sum_{i=1}^{\infty} (\lambda_i^s)^2 \phi_i(t)\phi_i(u), \qquad T_i \leq t, u \leq T_f, \end{aligned} \tag{131}$$

then

$$l_R^{(2)} = -\frac{1}{2}\left(\frac{2}{N_0}\right)^3 \int_{T_i}^{T_f}\int r(t)K_s^{(2)}(t, u)r(u)\, dt\, du. \tag{132}$$

Similarly, when $2\lambda_{\max}/N_0 < 1$, we can expand l_B. From (2.33),

$$\begin{aligned} l_B &= -\frac{1}{2}\sum_{i=1}^{\infty} \ln\left(1 + \frac{2}{N_0}\lambda_i^s\right) \\ &= -\frac{1}{2}\left\{+\frac{2}{N_0}\sum_{i=1}^{\infty}\lambda_i^s - \frac{1}{2}\left(\frac{2}{N_0}\right)^2 \sum_{i=1}^{\infty}(\lambda_i^s)^2 + \frac{1}{3}\left(\frac{2}{N_0}\right)^3 \sum_{i=1}^{\infty}(\lambda_i^s)^3 + \cdots\right\}. \end{aligned} \tag{133}$$

When $2\lambda_{\max}/N_0 \ll 1$, we can obtain an approximate expression by using the first *two* terms.

$$\begin{aligned} l_B &\simeq -\frac{1}{2}\left(\frac{2}{N_0}\right)\sum_{i=1}^{\infty}\lambda_i^s + \frac{1}{4}\left(\frac{2}{N_0}\right)^2 \sum_{i=1}^{\infty}(\lambda_i^s)^2 \\ &= -\frac{1}{2}\left(\frac{2}{N_0}\right)\int_{T_i}^{T_f} K_s(t, t)\, dt + \frac{1}{4}\left(\frac{2}{N_0}\right)^2 \int_{T_i}^{T_f}\int K_s^2(t, u)\, dt\, du. \end{aligned} \tag{134}$$

Equations (129), (132), and (134) correspond to two parallel operations on the received data and a bias term.

We can show that as

$$\frac{2}{N_0}\lambda_{\max}^s \to 0. \tag{135}$$

the ratio of the variance of $l_R^{(1)} + l_R^{(2)}$ on H_0 to the variance of $l_R^{(1)}$ on H_0 approaches zero. The same statement is true on H_1 because

$$\text{Var}\,[l_R^{(1)} \mid H_1] \simeq \text{Var}\,[l_R^{(1)} \mid H_0] \tag{136}$$

and

$$\text{Var}\,[l_R^{(2)} \mid H_1] \simeq \text{Var}\,[l_R^{(2)} \mid H_0]. \tag{137}$$

In this case, we may replace $l_R^{(2)}$ by its mean on H_0 (the means under both hypotheses are approximately equal):

$$E[l_R^{(2)} \mid H_0] = -\frac{1}{2}\left(\frac{2}{N_0}\right)^2 \int_{T_i}^{T_f}\int K_s^2(t, u)\, dt\, du. \tag{138}$$

Now $l_R^{(2)}$ becomes a bias term and $l_R^{(1)}$ is the only quantity that depends on $r(t)$. The resulting test is

$$l_R^{(1)} + l_B \simeq \frac{1}{2}\left(\frac{2}{N_0}\right)^2 \int_{T_i}^{T_f}\int r(t)K_s(t, u)r(u)\, dt\, du$$
$$- \frac{1}{2}\left(\frac{2}{N_0}\right)\int_{T_i}^{T_f} K_s(t, t)\, dt - \frac{1}{4}\left(\frac{2}{N_0}\right)^2 \int_{T_i}^{T_f}\int K_s^2(t, u)\, dt\, du. \tag{139}$$

Including the bias in the threshold gives the test

$$\boxed{\frac{1}{2}\left(\frac{2}{N_0}\right)^2 \int_{T_i}^{T_f}\int r(t)K_s(t, u)r(u)\, dt\, du \underset{H_0}{\overset{H_1}{\gtrless}} \gamma,} \tag{140}$$

where

$$\gamma = \ln \eta + \frac{1}{2}\left(\frac{2}{N_0}\right)\int_{T_i}^{T_f} K_s(t, t)\, dt + \frac{1}{4}\left(\frac{2}{N_0}\right)^2 \int_{T_i}^{T_f}\int K_s^2(t, u)\, dt\, du. \tag{141}$$

We refer to the receiver that performs the test in (140) as an optimum LEC receiver. Observe that it has exactly the same form as the general receiver in (124). The difference is that the kernel in the quadratic form is the signal covariance function instead of the optimum linear filter. Notice that the optimum linear filter reduces to $K_s(t, u)$ under the LEC condition. One form of the receiver is shown in Fig. 4.21. The various other realizations discussed in Section 2.1 (Figs. 2.4–2.7) can be modified for the LEC case.

When $2\lambda_{\max}^s/N_0$ is less than 1 but does not satisfy (128), we can use more terms in the series of l_R and l_B. As long as

$$\frac{2}{N_0}\lambda_{\max}^s < 1, \tag{142}$$

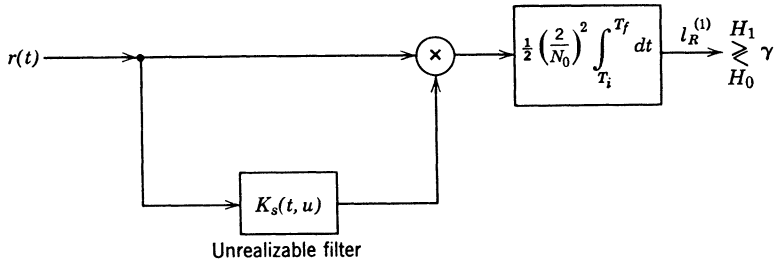

Fig. 4.21 Optimum LEC receiver.

we can find a series solution for the optimum detector that will converge.†

The general form follows easily,

$$l_R = -\frac{1}{2}\left(\frac{2}{N_0}\right)\int_{Ti}^{T_f} dt\, r(t) \sum_{n=1}^{\infty}\left(\frac{-2}{N_0}\right)^n \int_{T_i}^{T_f} K_s^{(n)}(t, u) r(u)\, du \tag{143}$$

and

$$l_B = \frac{1}{2}\sum_{n=1}^{\infty}\frac{1}{n}\left(-\frac{2}{N_0}\right)^n \int_{T_i}^{T_f} K_s^{(n)}(t, t)\, dt, \tag{144}$$

where

$$K_s^{(n)}(t, u) = \int_{T_i}^{T_f}\cdots\int_{T_i}^{T_f} K_s(t, z_1)K_s(z_1, z_2)\cdots K_s(z_{n-1}, u)\, dz_1 \cdots dz_{n-1}. \tag{145}$$

An interesting physical interpretation of higher-order approximations is given in Problem 4.3.2.

The final question of interest is the performance of the optimum receiver in the LEC case. We want to find a simpler expression for $\mu(s)$ by exploiting the smallness of the eigenvalues. From (2.134),

$$\mu(s) = \tfrac{1}{2}\sum_{i=1}^{\infty}[(1 - s)\ln(1 + 2\lambda_i^s/N_0) - \ln(1 + (1 - s)2\lambda_i^s/N_0)]. \tag{146}$$

Expanding the logarithms and retaining the first *two* terms, we have

$$\mu(s) \simeq \frac{1}{2}\sum_{i=1}^{\infty}\left\{(1 - s)\left[\frac{2}{N_0}\lambda_i^s - \frac{1}{2}\left(\frac{2}{N_0}\right)^2(\lambda_i^s)^2\right] - \left[(1 - s)\frac{2}{N_0}\lambda_i^s - \frac{(1 - s)^2}{2}\left(\frac{2}{N_0}\right)^2(\lambda_i^s)^2\right]\right\}. \tag{147}$$

We see that the terms linear in λ_i^s cancel. Writing $\sum_{i=1}^{\infty}(\lambda_i^s)^2$ in closed

† This approach to finding the filter is identical with trying to solve the integral equation iteratively using a Neumann series (e.g., Middleton [5] or Helstrom [4]). This procedure is a standard technique for solving integral equations.

form, we obtain

$$\mu(s) \simeq -\frac{s(1-s)}{2}\left\{\frac{1}{2}\left(\frac{2}{N_0}\right)^2 \int_{T_i}^{T_f}\int K_s^2(t, u)\, dt\, du\right\} \triangleq \mu_{\mathrm{LEC}}(s). \tag{148}$$

The term in braces has an interesting interpretation. For the *known* signal problem, we saw in Chapter I-4 that the performance was completely determined by d^2, where

$$d^2 \triangleq \frac{(E[l_R^{(1)} \mid H_1] - E[l_R^{(1)} \mid H_0])^2}{\mathrm{Var}\,[l_R^{(1)} \mid H_0]}. \tag{149}$$

Physically, this could be interpreted as the output signal-to-noise ratio. For the Gaussian signal problem discussed in this chapter, d^2 is no longer uniquely related to the error performance, because $l_R^{(1)}$ is *not* Gaussian. However, in the coherently undetectable case, it turns out that the term in braces in (148) is d^2, so that whenever our approximations are valid, the output signal-to-noise ratio leads directly to the approximate expressions for P_F, P_M, and Pr (ϵ). It remains to be verified that the term in braces in (148) equals d^2. This result follows easily by using the fact that the expectation of four jointly Gaussian random variables can be written as sums of second moments (e.g., [8, page 168] or page I-229). (See Problem 4.3.4.)

Thus, for the LEC case,

$$\mu_{\mathrm{LEC}}(s) = -\frac{s(1-s)}{2}\, d^2. \tag{150}$$

Substituting the expression for $\mu_{\mathrm{LEC}}(s)$ given in (150) into (2.164) and (2.173) gives the desired error expressions as

$$P_F \simeq \mathrm{erfc}_*\,(sd) = \mathrm{erfc}_*\left(\frac{d}{2} + \frac{\gamma}{d}\right) \tag{151}$$

$$P_M \simeq \mathrm{erfc}_*\,((1-s)d) = \mathrm{erfc}_*\left(\frac{d}{2} - \frac{\gamma}{d}\right). \tag{152}$$

The ROC obtained by varying the threshold γ is plotted in Fig. I-4.13.

The low-energy-coherence condition occurs frequently in radar astronomy and sonar problems. Price has studied the first area extensively (e.g., [6]), and we shall look at it in more detail in Chapter 11. In the sonar area the stationary process–long observation time assumption is often valid in addition to the LEC condition. The receiver and the performance are obtained by combining the results of this section with those in Section

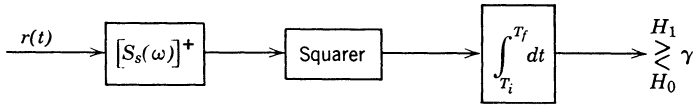

Fig. 4.22 Optimum receiver, low-energy-coherence, stationary-process, long-observation-time case.

4.1. A filter-squarer implementation of the resulting receiver is shown in Fig. 4.22. The value of d^2 is

$$\boxed{d^2 = \frac{T}{2}\left(\frac{2}{N_0}\right)^2 \int_{-\infty}^{\infty} S_s^2(\omega)\,\frac{d\omega}{2\pi}.} \tag{153}$$

We see that d^2 increases linearly with T, the observation time. Thus, regardless of the relative signal and noise levels, we can achieve a desired performance by observing the process over a sufficiently long observation time. We shall discuss the sonar area in more detail in *Array Processing*.

Occasionally the LEC receiver in Fig. 4.21 is used even though the LEC condition in (128) is not satisfied. In order to analyze the performance, we must treat it as a suboptimum receiver. In Chapter 5 we discuss performance analysis techniques for suboptimum receivers.

4.4 SUMMARY

In this chapter we have developed techniques for finding the optimum receiver and evaluating its performance for three special categories of detection problems. In Chapter 2, we had demonstrated a solution algorithm for cases in which the processes had finite-state representations.

It appears that a large portion of the physical situations that we encounter can be approximated by one of these four special cases. When this is true, we can design the optimum receiver completely and analyze its performance.

4.5 PROBLEMS

P.4.1 Stationary Process, Long Observation Time (SPLOT)

Unless otherwise indicated, you should assume that the SPLOT condition is valid in all problems in this section.

Simple Binary Detection

Problem 4.1.1. Consider the model in (1). Assume that $s(t)$ is a Wiener process such that

$$K_s(t, u) = \sigma^2 \min [t, u]$$

and

$$s(0) = 0.$$

1. Find the optimum receiver.
2. Evaluate $\mu_\infty(s)$ by using (20).
3. Compare your result with that in Problem 2.1.5.

Problem 4.1.2. Consider the expression for the logarithm of the Fredholm determinant given in (2.75).

1. Derive the asymptotic version of (2.75).
2. Use the result in part 1 to obtain an alternative expression for $\mu_\infty(s)$.
3. Evaluate $\mu_\infty(s)$ for the model in Problem 4.1.1.

Problem 4.1.3. Consider the model in (1). Assume that

$$S_s(\omega) = \frac{2nP}{k} \frac{\sin(\pi/2n)}{1 + (\omega/k)^{2n}}.$$

Evaluate $\mu_\infty(s)$ for this case.

Problem 4.1.4 (continuation). In Problem 4.1.3 we derived an expression for $\mu_\infty(s)$. Fix s at some value s_0, where

$$0 < s_0 < 1.$$

Study the behavior of $\mu_\infty(s_0)$ as a function of n. Consider different values of s_0. How does

$$\Lambda_B \triangleq \frac{2\pi P}{kN_0}$$

enter into the discussion?

Problem 4.1.5 (non-zero means). Consider the simple binary detection problem with nonzero means.

1. Derive the asymptotic version of (2.32) and (2.34).
2. Derive the asymptotic version of (2.147).

General Binary Detection

Problem 4.1.6. Consider the binary symmetric bandpass version of the class A_w problem. Assume that the equivalent low-pass signal spectrum is

$$S_{s_L}(\omega) = \frac{2nP_{LP}}{k} \frac{\sin(\pi/2n)}{1 + (\omega/k)^{2n}},$$

where

$$P_{LP} = \frac{P}{2}.$$

Recall that

$$\mu_{BS,BP,\infty}(\tfrac{1}{2}) = 4\mu_{SIB,LP,\infty}(\tfrac{1}{2}).$$

1. Use the result of Problem 4.1.3 to find $\mu_{BS,BP,\infty}(\frac{1}{2})$.
2. Express your answer in the form

$$\mu_{BS,BP,\infty}(\tfrac{1}{2}) \triangleq -\frac{E_r}{N_0} \cdot 4g_{BP,n}(\Lambda_B).$$

Plot $g_{BP,n}(\Lambda_B)$ for various n. Find

$$\max_{\Lambda_B} \left[g_{BP,n}(\Lambda_B) \right].$$

3. Find

$$\max_{n}\left\{\max_{\Lambda_B}\left[g_{BP,n}(\Lambda_B)\right]\right\}$$

Problem 4.1.7. Consider the binary symmetric bandpass version of the class A_w problem.

1. Write $\mu_{BS,BP,\infty}(1/2)$ as a function of $S_{s_L}(\omega)$ (the equivalent low-pass spectrum) and $N_0/2$.
2. Constrain

$$\int_{-\infty}^{\infty} S_{s_L}(\omega)\frac{d\omega}{2\pi} = \frac{P}{2}. \tag{P.1}$$

Find the spectrum that minimizes $\mu_{BS,BP,\infty}(1/2)$ subject to the constraint in (P.1).

Problem 4.1.8. Consider the class B problem (see Fig. 3.1). Verify that the results in Tables 4.1 and 4.2 are correct.

Problem 4.1.9. Consider the class B_w problem in which

$$S_s(\omega) = \frac{2kP_s}{\omega^2 + k^2}$$

$$S_n(\omega) = \frac{2k_1P_n}{\omega^2 + k_1^2}$$

$$S_w(\omega) = \frac{N_0}{2}.$$

1. Find the optimum receiver.
2. Evaluate $\mu_\infty(s)$.
3. Consider the special case in which $k_1 = k$. Simplify the expressions for $\mu_\infty(s)$.

Comment: In the discussion of minimum Pr (ϵ) tests in the text, we emphasized the case in which the hypotheses were equally likely and $\mu(s)$ was symmetric around $s = \frac{1}{2}$ (see pages 77–79). In many minimum Pr (ϵ) tests the hypotheses are equally likely but $\mu(s)$ is not symmetric. We must then solve the equation

$$\dot{\mu}(s)\big|_{s=s_m} = 0 \tag{F.1}$$

for s_m. We then use this value of s_m in (I-2.484) or (I-2.485). From the latter,

$$\Pr(\epsilon) \simeq \frac{1}{[2(2\pi\ddot{\mu}(s_m))^{\frac{1}{2}}s_m(1-s_m)]}\exp\mu(s_m). \tag{F.2}$$

(Assumes $s_m\sqrt{\ddot{\mu}(s_m)} > 3$ and $(1-s_m)\sqrt{\ddot{\mu}(s_m)} > 3$.) From (I-2.473),

$$\Pr(\epsilon) \leq \tfrac{1}{2}\exp\mu(s_m). \tag{F.3}$$

The next several problems illustrate these ideas.

Problem 4.1.10. Consider the class A_w problem in which

$$S_{s_1}(\omega) = \frac{2k\alpha P,}{\omega^2 + k^2},$$

$$S_{s_0}(\omega) = \frac{2kP}{\omega^2 + k^2}.$$

1. Draw a block diagram of the optimum receiver. Include the necessary biases.
2. Evaluate $\mu_\infty(s)$.
3. Assume that a minimum Pr (ϵ) test is desired and that the hypotheses are equally likely. Find s_m such that
$$\dot{\mu}(s)|_{s=s_m} = 0.$$
4. Compute the approximate Pr (ϵ) using (F.2).
5. Compute a bound on the Pr (ϵ) using (F.3).
6. Plot $\mu(s_m)$ as a function of α.
7. Evaluate
$$\left.\frac{\partial \mu_\infty(s, \alpha)}{\partial \alpha}\right|_{\alpha=0}.$$

This result will be useful when we study parameter estimation.

Problem 4.1.11. Consider the class A_w problem in which

$$S_{s_1}(\omega) = \begin{cases} \dfrac{\pi\alpha P}{k}, & |\omega| \leq k, \\ 0, & |\omega| > k, \end{cases}$$

and

$$S_{s_0}(\omega) = \begin{cases} \dfrac{\pi P}{k}, & |\omega| \leq k, \\ 0, & |\omega| > k. \end{cases}$$

Repeat Problem 4.1.10.

Problem 4.1.12. Consider the class A_w problem in which

$$S_{s_1}(\omega) = \frac{2\beta P_1}{\omega^2 + \beta^2}$$

and

$$S_{s_0}(\omega) = \frac{2\alpha P_0}{\omega^2 + \alpha^2}.$$

1. Repeat parts 1–5 of Problem 4.1.10.
2. Evaluate the approximate Pr (ϵ) for the case in which
$$\frac{\beta P_1}{\alpha P_0} = 1$$
and
$$N_0 = 0.$$

Problem 4.1.13. Consider the binary symmetric class A_w problem. All processes are symmetric around their respective carriers (see Section 3.4.3 and Fig. 3.9). The received waveform $r_{c_1}(t)$ is

$$\begin{aligned} r_{c_1}(t) &= s_{c_1}(t) + n_{c_1}(t) + w(t), \qquad T_i \leq t \leq T_f, \\ r_{c_1}(t) &= n_{c_1}(t) + w(t), \qquad T_i \leq t \leq T_f. \end{aligned} \tag{P.1}$$

Notice that (P.1) completely describes the problem because of the assumed symmetries. The random processes in (P.1) are statistically independent with spectra $S_s(\omega)$, $S_{n_c}(\omega)$, and $N_0/2$, respectively.

1. Derive a formula for $\mu_{\mathrm{BS,BP},\infty}(\frac{1}{2})$.
2. Assume that $S_s(\omega)$ and $N_0/2$ are fixed. Constrain the power in $n_{c_1}(t)$,

$$\int_{-\infty}^{\infty} S_{n_c}(\omega)\frac{d\omega}{2\pi} = \frac{P_c}{2}.$$

Choose $S_{n_c}(\omega)$ to *maximize* $\mu_{\mathrm{BP,BS},\infty}(\frac{1}{2})$.

3. Assume that $S_{n_c}(\omega)$ and $N_0/2$ are fixed. Constrain the power in $s_{c_1}(t)$,

$$\int_{-\infty}^{\infty} S_s(\omega)\frac{d\omega}{2\pi} = \frac{P_s}{2}.$$

Choose $S_s(\omega)$ to *minimize* $\mu_{\mathrm{BP,BS},\infty}(\frac{1}{2})$.

Problem 4.1.14. Consider the vector problem described in Problem 3.2.7. Specialize the results of this problem to the case in which the SPLOT condition is valid.

Problem 4.1.15. Consider the special case of Problem 4.1.14 in which

$$\mathbf{s}_1(t) = \int_{-\infty}^{\infty} \mathbf{h}(t-\tau)s(\tau)\,d\tau \tag{P.1}$$

and

$$\mathbf{s}_0(t) = \mathbf{0}. \tag{P.2}$$

The matrix filter $\mathbf{h}(\tau)$ has one input and N outputs. Its transfer function is $\mathbf{H}(j\omega)$. Simplify the receiver in Problem 4.1.14.

Problem 4.1.16. Consider Problem 3.2.8. Specialize the results to the SPLOT case.

Problem 4.1.17.

1. Consider Problem 3.2.9. Specialize the results to the SPLOT case.
2. Consider the particular case described in (P.1) of Problem 4.1.15. Specialize the results of part 1.

Problem 4.1.18.

1. Review the results in Problem 3.5.18. Derive an expression for $\mu_\infty(s)$ for the general vector case.
2. Specialize the result in part 1 to the class A_w SPLOT problem.
3. Specialize the results in part 2 to the class B_w SPLOT problem.
4. Specialize the results in part 1 to the case in which the signal is described by (P.1) in Problem 4.1.15.

Problem 4.1.19. The received waveforms on the two hypotheses are

$$r(t) = s_1(t) + w(t), \qquad T_i \le t \le T_f : H_1,$$

$$r(t) = s_0(t) + w(t), \qquad T_i \le t \le T_f : H_0.$$

The signals $s_1(t)$ and $s_0(t)$ are stationary, zero-mean, *bandpass* Gaussian processes centered at ω_1 and ω_0, respectively. Their spectra are disjoint and are *not* necessarily symmetric around their carrier frequencies. The additive noise is white $(N_0/2)$.

Find the optimum receiver and an expression for $\mu_{\mathrm{BP},\infty}(s)$. (*Hint:* Review the results of Problem 3.4.9.)

Problem 4.1.20. Consider the binary symmetric bandpass problem in Fig. 3.9. Assume that

$$E[r_{c_1}(t) \mid H_1] = m,$$

$$E[r_{c_0}(t) \mid H_0] = m.$$

All other means are zero.

1. Find the optimum receiver using the SPLOT assumption.
2. Evaluate $\mu_{\mathrm{BS,BS},\infty}(\frac{1}{2})$.

Problem 4.1.21. Consider the expression for $\mu(s)$ given in (2.208) and the expression for $\mu_\infty(s)$ given in (30).

1. Prove

$$\lim_{kT\to\infty} \mu(s) = \mu_\infty(s).$$

2. Consider the binary symmetric bandpass version of (2.208) and (30) [see Example 3, (59) and (60)]. Denote the BS, BP version of (2.208) as $\mu_{\mathrm{BS,BP}}(s, kT)$. Plot

$$f(kT) \triangleq \frac{\mu_{\mathrm{BS,BP}}(1/2, kT) - \mu_{\mathrm{BS,BP},\infty}(\frac{1}{2})}{\mu_{\mathrm{BS,BP}}(1/2, kT)}$$

as a function of kT in order to study the accuracy of the SPLOT approximation.

P.4.2 Separable Kernels

Problem 4.2.1. Consider the pulsed radar problem. The performance is characterized by (98)–(102). From (101),

$$\mu_{\mathrm{BP,SK}}(s) = K \ln\left[\frac{(1 + \bar{E}_{r1}/N_0)^{1-s}}{1 + (1-s)\bar{E}_{r1}/N_0}\right].$$

Choosing a particular value of s corresponds to choosing the threshold in the LRT.

1. Fix $s = s_m$ and require

$$\mu(s_m) - s_m\dot{\mu}(s_m) = c.$$

Constrain

$$\bar{E}_r = K\bar{E}_{r1}.$$

Choose K to minimize

$$F \triangleq \mu(s_m) + (1 - s_m)\dot{\mu}(s_m).$$

Explain the physical significance of this procedure.

2. Compare the results of this minimization with the results in Figs. 4.17 and 4.18.

Problem 4.2.2.

1. Consider the separable kernel problem in which the a_i in (89) have non-zero means a_i. Find $\mu_D(s)$.
2. Consider the bandpass version of the model in part 1. Assume that each successive pair of a_i have identical statistics. Evaluate $\mu_D(s)$ and $\mu_R(s)$.

Problem 4.2.3.

1. Consider the binary symmetric version of the bandpass model in Problem 4.2.2. Evaluate $\mu_{\mathrm{BS,BP,SK}}(\frac{1}{2})$.

2. Simplify the results in part 1 to the case in which all of the a_i are identically distributed. Assume

$$E[a_i] = m$$

and

$$\text{Var}\,[a_i] = \sigma_s^2.$$

Problem 4.2.4. Consider the model in Problem 4.2.3. A physical situation in which we would encounter this model is a frequency diversity system operation over a Rician channel (see Section 4.2.2). If the energy in the transmitted signal is E_t, then

$$m^2 = \alpha E_t,$$

$$\sigma_s^2 = \beta E_t,$$

where α and β are the strengths of the specular path and the random path, respectively.

1. Express $\mu_{\text{BS,BP,SK}}(1/2)$ in terms of α, β, E_t, and K (the number of paths).

2. Assume that E_t is fixed. Choose K to minimize $\mu_{\text{BS,BP,SK}}(\frac{1}{2})$. Explain your results intuitively and compare them with (116).

Problem 4.2.5. Consider the diversity system described in Section 4.2.2. If the signal eigenvalues were different, we could write the efficiency factor in (114) as

$$g_d(\boldsymbol{\lambda}) = \sum_{i=1}^{K} \frac{1}{2\lambda_i} \ln \left\{ \frac{(1 + \lambda_i/2)^2}{(1 + \lambda_i)} \right\}. \tag{P.1}$$

Assume

$$\sum_{i=1}^{K} \lambda_i = c. \tag{P.2}$$

You may choose K and λ_i subject to the restriction in (P.2). Prove that $g_d(\boldsymbol{\lambda})$ is maximized by the choice

$$\lambda_i = \begin{cases} \lambda, & i = 1, 2, \ldots, K_0, \\ 0, & i > K_0. \end{cases}$$

Find K_0.

Problem 4.2.6 Consider the frequency diversity system operating over a Rayleigh channel as described in Section 4.2.

1. Generalize the model to allow for unequal path strengths, unequal energy transmitted in each channel, and unequal noise levels.

2. Consider the two-channel problem. Constrain the total transmitted power. Find the optimum division of energy to minimize $\mu_{\text{BS,BP,SK}}(1/2)$.

Problem 4.2.7. Consider the class A_w problem in which

$$K_{s_1}(t, u) = \sum_{i=1}^{N_1} \lambda_i^{s_1} f_i(t) f_i(u), \qquad T_i \leq t, u \leq T_f$$

and

$$K_{s_0}(t, u) = \sum_{j=1}^{N_2} \lambda_j^{s_0} g_j(t) g_j(u), \qquad T_i \leq t, u \leq T_f, \tag{P.1}$$

where

$$\int_{T_i}^{T_f} f_i(t)f_k(t)\,dt = \delta_{ik}, \qquad i, k = 1, \ldots, N_1,$$

$$\int_{T_i}^{T_f} g_j(t)g_k(t)\,dt = \delta_{jk}, \qquad i, k = 1, \ldots, N_2,$$

and

$$\int_{T_i}^{T_f} f_i(t)g_j(t)\,dt = \rho_{ij}, \qquad i = 1, \ldots, N_1, \quad j = 1, \ldots, N_2. \tag{P.2}$$

1. Solve (3.33) for $h_\Delta(t, u)$.
2. Specialize part 1 to the case in which

$$\rho_{ij} = 0, \qquad i = 1, \ldots, N_1, \quad j = 1, \ldots, N_2. \tag{P.3}$$

Explain the meaning of (P.3). Give a physical situation in which (P.3) is satisfied.

3. Derive a formula for $\mu_{SK}(s)$.
4. Specialize the result in part 3 to the case in which (P.3) is satisfied.

Problem 4.2.8. Consider the class B_w problem in which the received waveforms on the two hypotheses are

$$r(t) = s(t) + w(t), \qquad T_i \leq t \leq T_f : H_1,$$
$$r(t) = w(t), \qquad T_i \leq t \leq T_f : H_0.$$

The signal and noise processes are statistically independent, zero-mean processes with covariance functions $K_s(t, u)$ and $N_0\,\delta(t - u)/2$, respectively. The signal process $K_s(t, u)$ is separable and has M equal eigenvalues,

$$K_s(t, u) = \lambda_0 \sum_{i=1}^{M} \phi_i(t)\phi_i(u), \qquad T_i \leq t, u \leq T_f.$$

1. Verify that the receiver in Fig. P.4.1 is optimum.

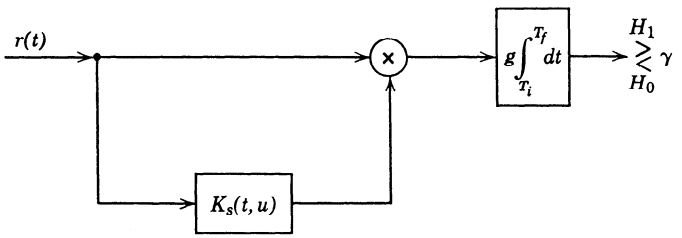

Fig. P.4.1

2. Compute g. Compare the receiver in Fig. P.4.1 with the LEC receiver of Section 4.3.

P.4.3 Low Energy Coherence (LEC)

Problem 4.3.1. Consider the development in (129)–(139). Verify that the various approximations made in arriving at (139) are valid.

Problem 4.3.2.

1. Verify the general form in (143).

2. An easy way to remember the structure of l_R in (143) is shown in Fig. P.4.2. This is an unrealizable feedback system. Verify that the output is l_R.

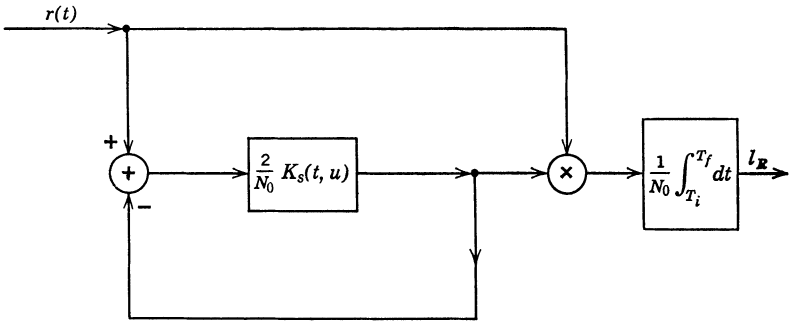

Fig. P.4.2

3. Why is the result in part 2 obvious? Is the receiver in Fig. P.4.2 optimum for the general case? Why is it a useful idea in the LEC case but not in the general case?

Problem 4.3.3. Consider the vector model in Problem 3.2.7, in which $\mathbf{s}_0(t) = \mathbf{0}$.

1. Find the optimum receiver under the LEC condition. Define precisely what the LEC condition is in the vector case.

2. Assume that both the SPLOT and LEC conditions hold. Find the optimum receiver and derive an expression for $\mu_{\infty,\mathrm{LEC}}(s)$. Express the LEC condition in terms of the signal spectral matrix $\mathbf{S}_1(\omega)$.

Problem 4.3.4. Derive the result in (149).

REFERENCES

[1] R. Price and P. E. Green, Jr., "Signal Processing in Radar Astronomy—Communication via Fluctuating Multipath Media," Massachusetts Institute of Technology, Lincoln Laboratory, Technical Report 234, October 1960.

[2] R. Price, "Detectors for Radar Astronomy," in *Radar Astronomy*, J. V. Evans and T. Hagfors Eds., New York, McGraw-Hill, 1968.

[3] D. Middleton, "On Singular and Nonsingular Optimum (Bayes) Tests for the Detection of Normal Stochastic Signals in Normal Noise," IRE Trans. **IT-7**, No. 2, 105–113 (April 1961).

[4] C. W. Helstrom, *Statistical Theory of Signal Detection*, Pergamon Press, New York, 1960.

[5] D. Middleton, *An Introduction to Statistical Communication Theory*, McGraw-Hill, New York, 1960.

[6] R. Price, "Output Signal-to-Noise Ratio as a Criterion in Spread-Channel Signaling," Massachusetts Institute of Technology, Lincoln Laboratory, Technical Report 388, May 13, 1965.

[7] D. Middleton, "On the Detection of Stochastic Signals in Additive Normal Noise," IRE Trans. **PGIT-3,** 86–121 (1957).

[8] W. B. Davenport and W. L. Root, *Random Signals and Noise*, McGraw-Hill, New York, 1958.

[9] D. Middleton, "Canonically Optimum Threshold Detection," IEEE Trans. Information Theory **IT-12,** No. 2, 230–243 (April 1966).

[10] J. Capon, "On the Asymptotic Efficiency of Locally Optimum Detectors," IRE Trans. Information Theory **IT-7,** 67–71 (April 1961).

[11] P. Rudnick, "Likelihood Detection of Small Signals in Stationary Noise," J. Appl. Phys. **32,** 140 (Feb. 1961).